



Title	Periodic Structure of an Ion-Related Vertical Instability in the KEK Photon Factory Electron Storage Ring
Author(s)	持箸, 晃
Citation	大阪大学, 2001, 博士論文
Version Type	VoR
URL	https://doi.org/10.11501/3183827
rights	
Note	

The University of Osaka Institutional Knowledge Archive : OUKA

<https://ir.library.osaka-u.ac.jp/>

The University of Osaka

Periodic Structure of an Ion-Related Vertical
Instability in the KEK Photon Factory
Electron Storage Ring

Akira Mochihashi

Research Center for Nuclear Physics
Osaka University

2001

Abstract

In the KEK-PF electron storage ring, a vertical beam instability has been observed in a multi-bunch condition in which a series of bunches (a bunch train) followed by a series of empty buckets is stored. The instability depends on a vacuum condition in the ring; therefore, it seems to be an ion-related phenomenon. Because such a phenomenon causes a change in the betatron oscillation frequency (tune), it is essential to measure the tune to study the mechanism of the instability. We have developed an optical bunch-by-bunch beam diagnostic system which can observe the oscillations of individual bunches in the multi-bunch operation and have measured the vertical tune of the individual bunches with the system. We obtained the result that the tune rose in the head and fell in the tail of the bunch train. The classical theory of ion trapping describes the tune shift induced by trapped ions; however, the change in the tune along the train that we observed is not explained by the classical theory. On the other hand, Fast Beam-Ion Instability theory has treated the change in the tunes along the train; however, our experimental results don't agree with the theory quantitatively. Consequently, we tried a theoretical model that gives a modulation of the ion density along the train, and estimated a theoretical value of the change in the tunes along the train. The agreement between our experimental results and the theoretical prediction was quite good.

Acknowledgments

I would like to express my sincere thanks to Professor K. Sato for providing me that the opportunity to study the beam dynamics in circular accelerators as my doctoral thesis.

It is my great honor to acknowledge Professor T. Kasuga of KEK for helpful discussion and continuous encouragement throughout this work.

I would like to show appreciation to Dr. T. Obina and Mr. Y. Tanimoto of KEK for their kind assistance throughout the experiments and the theoretical analyses. I would like to acknowledge to Professor M. Kobayashi and staffs of the light source division of KEK Photon Factory who have been kindly supporting the experiments.

I would like to show appreciation to Dr. S. Ninomiya of Osaka university for his supports and useful suggestions.

I wish to thank to Research Fellowships of the Japan Society for the Promotion of Science for Young Scientists for its financial support.

Contents

1	Introduction	4
2	Theory	9
2.1	Change in Tunes along Bunch Train	
	Due to Modulation of Ion Density	9
2.1.1	Ion Motion	10
2.1.2	“Ion Twiss Parameters”	12
2.1.3	Tune Shift due to Trapped Ions	13
2.2	Fast Beam-Ion Instability (FBII)	15
3	Observations	17
3.1	High-Speed Light Shutter	17
3.1.1	Principles of High-Speed Light Shutter	18
3.1.2	Operation of High-Speed Light Shutter	18
3.2	Detection of Betatron Oscillation of Individual Bunches with Optical Method	20
4	Results	22
4.1	Change in Tunes	22
4.1.1	Measurement and Analysis of Tunes	22
4.1.2	Correction of Dependence of Tunes on Beam Current	23

4.1.3	Change in Tunes in Head of Bunch Train	24
4.2	Change in Amplitude	25
5	Discussion	26
5.1	Change in Tunes	26
5.1.1	Long Bunch Train	26
5.1.2	Short Bunch Trains	29
5.2	Change in Amplitudes	30
6	Conclusion	31
A	Ion Trapping	34
A.1	Ion Motion	34
A.2	Tune Shift	36
B	Twiss Parameters	38
B.1	Definition of Twiss Parameters	38
B.2	Particle Motion with Twiss Parameters	39
C	High-Speed Light Shutter	41
D	Laslett Tune Shift	44

Chapter 1

Introduction

An electron beam in a storage ring is designed to follow a closed orbit that is determined by magnetic guide fields produced by bending dipole magnets and focusing quadrupole magnets. Because an electron experiences a periodic force in the storage ring, it oscillates around the closed orbit. This oscillation is called a betatron oscillation and the number of oscillations in one revolution in the ring is called the betatron number or tune. Since horizontal and vertical motions can be treated independently, the average storage ring has horizontal and vertical tunes. The tunes are determined by the lattice, i.e., the configuration of the magnets of the ring. However, the tunes can vary from the designed values because of many reasons, and the change in the tunes is called a tune shift. An ion-trapping effect and electromagnetic fields induced by the beam itself are examples of major sources of tune shifts.

Highly relativistic electrons moving in a circular orbit emit photons in the tangential direction. This phenomenon is known as synchrotron radiation (SR) with a wide-wavelength from infrared to X-ray. An RF acceleration system used to compensate for the energy loss due to SR produces stable areas called RF buckets around the synchronous phases at which the energy

gain is equal to the energy loss. In these buckets, electrons form clusters, called bunches, the maximum number of which is determined by the number of RF wavelengths around the ring circumference, namely, the harmonic number.

A storage ring is always kept in an ultra-high vacuum condition (~ 50 nPa on average) in order to keep the lifetime of the stored beam large enough. However, the electron beam collides with residual gas molecules and creates positive ions when the beam passes through a vacuum system. The ions are attracted and trapped by the electron beam, and, consequently, the beam passes through “ion-clouds”. The beam is affected by the Lorentz force due to the ion-clouds, and the original motion of the beam can be affected. This phenomenon is called an ion-trapping effect [1, 2], and can cause the tune shift. Because the ion-clouds induce focusing fields on the beam, the ion-trapping effect has a tendency to increase the tunes. On the other hand, a space charge of the beam itself can also cause the tune shifts. This phenomenon is well known and called a Laslett tune shift [3].

In the Photon-Factory electron storage ring (PF-ring) at the Institute of Materials Structure Science, High Energy Accelerator Research Organization (KEK), a vertical beam instability has been observed in a multi-bunch condition in which a series of bunches (a bunch train) followed by a series of empty buckets (bunch gaps) are stored in the ring. The instability can be suppressed by exciting octupole magnets in routine operation; however, the origin of the phenomenon has not been perfectly understood yet. The instability depends on the condition of the vacuum in the ring; namely, the instability is observed under poor vacuum conditions and becomes weak in good vacuum conditions. In addition, the instability was enhanced after the

emittances of the PF-ring was improved in 1998. We claim that (a) the dependence of the instability in the PF-ring on the vacuum conditions implies that the phenomenon was ion-related, and (b) the fact that the instability is enhanced after the decrease of the emittances implies that the size of the ion-clouds became small with the decrease of the emittances and, consequently, the ion density around the beam increased, strengthening the electric fields due to the ion-clouds. However, this phenomenon has not been sufficiently characterized up to now.

To observe the instability, we have developed a bunch-by-bunch beam diagnostic system which can observe the oscillations of individual bunches in the multi-bunch operation. The system can pick out a light pulse from a certain bunch in a train of light pulses from many bunches, and observe the tunes of the individual bunches by detecting the spatial oscillation of the light. Using the system, we observed spontaneous betatron oscillations and measured the vertical tunes of the individual bunches. We found that the tunes rose in the head and fell in the tail of the train.

The change in the tunes along the bunch train seems to be caused by an ion-related phenomenon. However, in the classical theory of ion trapping, [1, 2], in which the tune shifts induced by trapped ions are discussed, the change in the tunes along the train is not explained. In contrast, the Fast Beam-Ion Instability (FBII) theory [7] deals with the phenomenon in which the gas molecules are ionized during passage of the bunch train and the ions are trapped successively. In the situation, the ion density increases along the train, and accordingly, the tunes vary along the train. However, the FBII theory cannot explain the experimental result that the tunes rise in the head and fall in the tail. Moreover, the experimental results for the change in the tunes along the train does not agree with the FBII theory quantitatively.

We tried a theoretical model that gives the modulation of the ion density along the train by treating the ion motion with a method similar to the theory of the betatron oscillation in circular accelerators. We estimated the theoretical value of the change in the tunes along the train and compared it with the experimental results. The agreement between the theory and the experiment was quite good. We also performed other experiments with short bunch trains, and discussed them in light of this theory.

The motion of the ions trapped by the beam, and the theory of the modulation of the ion density, and the theory of the tune shifts along the bunch train are summarized in Chapter 2. The bunch-by-bunch beam diagnostic system and the observations with the system are described in Chapter 3. The experimental results and the discussions are described in Chapters 4 and 5, respectively. Conclusions are given in Chapter 6.

The main parameters of the PF-ring are summarized in Table 1.1. The symbols in the table are used without further notice.

Table 1.1: Main parameters of PF-ring.

Parameters	Symbol	Value
Beam energy	E	2.5 GeV
Circumference	C_0	187 m
RF frequency	f_{RF}	500.1 MHz
Revolution frequency	f_{rev}	1.60 MHz
Bunch spacing	t_{RF}	2.0 ns
Revolution period	t_{rev}	0.62 μ s
Harmonic number	h	312
Betatron tune	ν_x/ν_y	9.62/4.28

Chapter 2

Theory

2.1 Change in Tunes along Bunch Train Due to Modulation of Ion Density

An electron beam circulating in vacuum vessels of the storage ring collides with residual gas molecules and creates ions. Because the ions have a positive charge, they are attracted by an electric field induced by the beam. The ions which satisfy certain conditions ¹ are stably trapped around the beam orbit and induce electric fields. The beam is affected by a focusing force induced by the electric field due to the ion-cloud, and, consequently, a tune shift occurs. In such an ion-related phenomenon, tunes have a tendency to increase from the original values determined by the magnet system of the storage ring.

Because ions at a certain location in the storage ring are affected by a periodic focusing force with a period of t_{rev} corresponding to the configuration of the bunch train, ion motion can be discussed with a method similar to that for the betatron oscillation in circular accelerators. Namely, an “ion betatron

¹The stability condition of the trapped ion are discussed in Sec. 2.1.1.

function β_i ” with the period t_{rev} can be defined as a function of the time lapse τ from the passage of a bunch head. The vertical displacement y_i of the ion at time t is given by

$$y_i(t) = y_0 \sqrt{\beta_i(\tau)} \cos \phi(t), \quad (2.1)$$

where y_0 is a constant and $\phi(t)$ is the phase of the ion motion. Figure 1 defines τ and the location s in the ring.

Because trapped ions oscillate around the electron beam with amplitudes proportional to $\sqrt{\beta_i}$, the size of the ion-cloud is proportional to $\sqrt{\beta_i}$, and because $\sqrt{\beta_i}$ is a periodic function of τ , the density of the ions is a function of τ with a period of t_{rev} . According to the “classical” theory of ion trapping [1, 2], the trapped ions cause tune shifts proportional to their density. Therefore, the variation of the ion density could cause the tune shifts of bunches that depend on their positions in the train.

2.1.1 Ion Motion

The vertical displacement of the ion affected by the bunch train can be expressed in matrix form [2] by

$$\begin{aligned} \begin{pmatrix} y_i(t + t_{RF}) \\ \dot{y}_i(t + t_{RF}) \end{pmatrix} &= \begin{pmatrix} 1 & t_{RF} \\ 0 & 1 \end{pmatrix} \begin{pmatrix} 1 & 0 \\ a & 1 \end{pmatrix} \begin{pmatrix} y_i(t) \\ \dot{y}_i(t) \end{pmatrix} \\ &= DB \begin{pmatrix} y_i(t) \\ \dot{y}_i(t) \end{pmatrix}, \end{aligned} \quad (2.2)$$

where t_{RF} is the bunch spacing ($= 1/f_{RF}$) and a denotes an impulse due to the passage of one bunch:

$$a = -\frac{2r_p c N_b}{A\sigma_y (\sigma_x + \sigma_y)}, \quad (2.3)$$

where r_p the classical proton radius, c the speed of light, N_b the number of the electrons in the bunch, A the mass number of the ion, and σ_x, σ_y the horizontal and vertical beam sizes, respectively.²

In Eq. (2.2), the matrices B and D represent a thin-lens kick by a bunch and a drift between the bunches, respectively. The matrix for passage of the whole bunch train that consists of bunches with the same beam current can be written as the product of DB and D , namely,

$$\begin{aligned} \begin{pmatrix} y_i(t + t_{rev}) \\ \dot{y}_i(t + t_{rev}) \end{pmatrix} &= D^{h-n_b} (DB)^{n_b} \begin{pmatrix} y_i(t) \\ \dot{y}_i(t) \end{pmatrix} \\ &= M \begin{pmatrix} y_i(t) \\ \dot{y}_i(t) \end{pmatrix}, \end{aligned} \quad (2.4)$$

where n_b is the number of bunches in the train.

The stability of the ion motion can be discussed with a method similar to the theory of the betatron oscillation in circular accelerators. Namely, the stability condition for the ions can be written with the trace of the matrix M as [2]

$$\frac{1}{2} |\text{Tr } M| \leq 1. \quad (2.5)$$

Because the trace depends not only on the configuration of the bunch train but also on the beam size, the stability condition differs at different positions in the ring under the same configuration of the train.

We calculated the ratio of the total area of the regions where the ions are trapped to the area of the whole ring in various configurations of the train. The result is shown in Fig. 2. In the calculation we divided the PF-ring circumference into pieces each 10 cm long and estimated the stability of the ions in each piece. Then, we calculated the percentage of the regions

²The derivation of Eqs. (2.2) and (2.3) is discussed in Appendix A.

where the ions were trapped. Figure 2 shows with contour lines the ratio for various configurations of the train. In the calculation, an ion species of CO^+ , which is the main component of the residual gas molecules in the PF-ring, is assumed. As seen in the figure, ions are rarely trapped when the train length is shorter than 100 bunches and the bunch current is equal to 1.6 mA/bunch, the bunch current in routine operation.

2.1.2 “Ion Twiss Parameters”

Because ions are affected by the periodic focusing force corresponding to the configuration of the bunch train, “ion Twiss parameters”³ can be defined as a function of the time lapse τ from passage of the bunch head. The parameters at the n -th bunch in the train are written as

$$\begin{pmatrix} \beta_i(nt_{RF}) \\ \alpha_i(nt_{RF}) \\ \gamma_i(nt_{RF}) \end{pmatrix} = m_{bunch}^n \begin{pmatrix} \beta_i(0) \\ \alpha_i(0) \\ \gamma_i(0) \end{pmatrix}, \quad (2.6)$$

where $\beta_i(0)$, $\alpha_i(0)$, and $\gamma_i(0)$ are the parameters at the head of the bunch train, m_{bunch} is the 3×3 transformation matrix whose parameters are composed of matrix elements of DB [6]. Because the bunch train has a mirror symmetry around the center of the train, the betatron function of the ion, $\beta_i(\tau)$, is also mirror symmetric. Examples of β_i for a multi-bunch mode, in which a series of 280 bunches followed by a series of 32 empty buckets with a bunch current of 1.6 mA/bunch, are shown in Fig. 3. In the calculation of β_i , a CO^+ ion is assumed.

³The Twiss parameters are described in Appendix B.

2.1.3 Tune Shift due to Trapped Ions

In the classical theory of ion trapping, the size of an ion cloud is assumed to be equal to that of the beam. However, as discussed in the previous sections, the size of the ion-cloud is modulated by the passage of a bunch train. Considering the effect of the modulation, we assume that the horizontal/vertical size $\Sigma_{x,y}(\tau)$ of the ion-cloud is proportional to the horizontal/vertical beam sizes $\sigma_{x,y}$, and is time dependent; namely,

$$\Sigma_{x,y}(\tau) = \epsilon_{x,y}(\tau)\sigma_{x,y}, \quad (2.7)$$

where $\epsilon_{x,y}(\tau)$ is a factor which gives the time dependence but is independent of s .

If the ion-cloud is assumed to have a gaussian distribution, the vertical component of the electric field \mathcal{E}_y induced by the cloud under linear approximation is

$$\mathcal{E}_y(\tau) = \frac{e}{2\pi\epsilon_0} \frac{\eta\lambda_e}{\Sigma_y(\tau)(\Sigma_x(\tau) + \Sigma_y(\tau))} y, \quad (2.8)$$

where λ_e is the averaged line density of the electrons, η the neutralization factor, e the electron charge, and ϵ_0 the dielectric constant of the free space.

Because the beam size $\sigma_{x,y}$ depends on the location s in the storage ring, the electric field \mathcal{E}_y also depends on s . From Eq. (2.8), a vertical tune shift $\Delta\nu_y(\tau)$ caused by the trapped ions is given by

$$\begin{aligned} \Delta\nu_y(\tau) &= \frac{1}{4\pi} \int_C \frac{e}{E} \frac{\partial \mathcal{E}_y(\tau)}{\partial y} \beta_y ds \\ &= \frac{r_e E_0}{2\pi E} \lambda_e \eta \int_C \frac{\beta_y}{\Sigma_y(\tau)(\Sigma_x(\tau) + \Sigma_y(\tau))} ds, \end{aligned} \quad (2.9)$$

where E_0 is the rest mass of the electron, r_e the classical electron radius, and β_y the betatron function of the beam, not the function for the ions. The integral in Eq. (2.9) is taken over the area C where ions are stably trapped around the beam.

Now we rewrite Eq. (2.9) using Eq. (2.7):

$$\begin{aligned}\Delta\nu_y(\tau) &= \frac{r_e E_0}{2\pi E} \frac{\lambda_e \eta}{\epsilon_x(\tau)\epsilon_y(\tau)} \int_C \frac{\beta_y}{\sigma_y \left(\sigma_x + \frac{\epsilon_y(\tau)}{\epsilon_x(\tau)} \sigma_y \right)} ds \\ &\approx \frac{\Delta\nu_y^0}{\epsilon_x(\tau)\epsilon_y(\tau)},\end{aligned}\tag{2.10}$$

where $\Delta\nu_y^0$ is the tune shift in the classical theory of ion trapping [2]:

$$\Delta\nu_y^0 = \frac{r_e E_0}{2\pi E} \lambda_e \eta \int_C \frac{\beta_y}{\sigma_y (\sigma_x + \sigma_y)} ds.\tag{2.11}$$

Here, the horizontal motion of the ions is neglected because the horizontal beam size is larger than the vertical size. If we assume that the horizontal size of the ions equals the horizontal beam size, i.e., $\epsilon_x(\tau) = 1$, the tune shift along the bunch train is simply written as

$$\Delta\nu_y(\tau) = \frac{\Delta\nu_y^0}{\epsilon_y(\tau)}.\tag{2.12}$$

Because the impulse acting on the ions depends on the beam size where the ions are trapped, $\beta_i(\tau)$ depends on location in the ring. The size of the ion-cloud is proportional to $\sqrt{\beta_i(\tau)}$, and the ratio $1/\epsilon_y(\tau)$ is also proportional to an average of $1/\sqrt{\beta_i(\tau)}$ over the whole ring, namely,

$$\frac{1}{\epsilon_y(\tau)} = b_0 \int_C \frac{1}{\sqrt{\beta_i(\tau)}} ds,\tag{2.13}$$

where b_0 is a normalization constant which satisfies

$$\frac{1}{n_b t_{RF}} \int_0^{n_b t_{RF}} \frac{1}{\epsilon_y(\tau)} d\tau = 1.\tag{2.14}$$

We can estimate the tune shift along the bunch train due to the modulation of the ion density from Eq. (2.12) with Eq. (2.13). Figure 4 shows an example of the calculated tune shifts as a function of the bunch position in the train. In the calculation, the multi-bunch operation which corresponds

to the condition in Fig. 3 and a neutralization factor of 1.0×10^{-5} which is consistent with the measured value⁴ are assumed. In the figure, it is clearly seen that the tunes change along the train, and, in particular, they gradually rise in the head and fall in the tail.

2.2 Fast Beam-Ion Instability (FBII)

The ions created by the passage of the bunch can be trapped by the following bunches in the train successively. Because such a trapping phenomenon occurs even in a single passage of the bunch train, the phenomenon does not have a stability condition, in contrast with the classical ion trapping. The ions transiently trapped can disturb the original motion of the beam. Such a phenomenon is called the Fast Beam-Ion Instability (FBII) [7]. FBII theory assumes that there are no ions at the head of the bunch train. Therefore, in circular accelerators, the theory is valid in the case that all of the ions are cleared in a series of empty buckets (bunch gaps).

The FBII can also cause the change in tunes along the bunch train because the ion density increases along the bunch train by creation and trapping of the ions. The line density of the ions λ_i created by the passage of the bunches increases along the bunch train:

$$\lambda_i(\tau) = \sigma_i N_b \frac{P}{k_b T} \tau, \quad (2.15)$$

where σ_i is the ionization cross section, P and T the pressure and temperature of the residual gas, and k_b the Boltzmann constant, respectively. From Eq. (2.11), the change in tunes along the bunch train due to FBII is given by

$$\Delta \nu_y^{FBII}(\tau) = \frac{r_e E_0}{2\pi E} \lambda_i(\tau) \int_{C_0} \frac{\beta_y}{\sigma_y (\sigma_x + \sigma_y)} ds, \quad (2.16)$$

⁴Details about the neutralization factor are in Sec. 5.1.1.

where the integral in Eq. (2.16) is taken over the whole ring C_0 .

We calculated a change in tunes $\left(\frac{\Delta\nu_y}{\Delta n}\right)$ along the bunch train with Eq. (2.16). In the calculation, the ion species is assumed to be CO^+ and the ionization cross section to be 1.77 Mbarn, corresponding to the value for scattering between the CO and the electrons with an energy of 2.5 GeV [8]. We assumed a pressure of 7.5×10^{-8} Pa for the CO around the beam orbit that is 3 times as large as the measured partial pressure of the CO where the gauges are set [9]. From the calculation, we concluded that the change in tunes in the train due to FBII is $\frac{\Delta\nu_y}{\Delta n} \approx 1.8 \times 10^{-7}/\text{bunch}$.

Chapter 3

Observations

3.1 High-Speed Light Shutter

In order to observe phenomena that depend on position in the bunch train, it is necessary to detect the motion of the individual bunches in the train. An analog switching method, in which the multi-bunch signal from a beam monitor electrode is gated to single out a signal corresponding to a certain bunch, is usually adopted for such beam diagnostic systems. In the method, a gate-pulse with a pulse width shorter than a bunch spacing (2 ns in the PF-ring) is necessary. This bunch-by-bunch beam diagnostics with a fast analog switching method [10] has been applied to electronic detection with button-type beam position monitors (BPMs). However, ringing that commonly occurs in a fast electronic switch degraded the detection capability. Moreover, the electronic detection has an unavoidable problem that the BPMs detect not only the beam signal but also electromagnetic fields induced by the beam due to the discontinuities or the cavity-like structures of vacuum vessels.

To avoid these problems, we have adopted an optical beam detection method and developed an optical analog switch called a “high-speed light

shutter” [5]. Because the shutter can be opened or closed in the bunch spacing time, it can pick out a light pulse from an individual bunch in a light pulse train. Two of its merits is that the light shutter is free from harmful effects caused by ringing and it has an excellent tolerance to electronic noise. The basic principle of the high-speed light shutter and its basic operation are described in the following sections.

3.1.1 Principles of High-Speed Light Shutter

A schematic diagram of the shutter is shown in Fig. 5. A pockels cell (Fast-pulse Technology, 1044-FW) is placed between polarization filters whose polarization angles are perpendicular to each other. The incident light can pass through the shutter while a high voltage pulse is applied to the cell because the cell rotates the polarization plane. Since the time response of the cell is fast enough, the operation speed of the shutter is mainly determined by the rise and fall time of the pulser. The waveform of the output pulse of the pulser is shown in Fig. 6. The pulse has a width (FWHM) of about 1.7 ns, which is shorter than the bunch spacing of 2 ns, and a height of 550 V. We operate the shutter with a repetition rate of $f_{shutter} = 534$ kHz which corresponds to one third of the revolution frequency of the PF-ring because of the limitation of the repetition rate of the high voltage pulser (max. 600 kHz) and the reason described in Sec. 3.2.

3.1.2 Operation of High-Speed Light Shutter

Experiment with CW-laser

A block diagram of the high-speed light shutter, including the optical setup, is shown in Fig. 7. In order to observe the time structure of the shutter we

made use of a photon counting method [11, 12] and used a CW-laser (Spectra Physics, $\lambda = 488$ nm) as a light source. To improve the polarization of the incident light on the cell we used two polarizers. A signal generator generates a signal with a frequency equal to f_{RF} in the PF-ring. A divider generates a signal with a repetition frequency of $f_{rev}/3 = 534$ kHz. We used the signal as a trigger for the high voltage pulser.

The light through the shutter passes through a pair of lenses. To eliminate stray light due to multiple scattering between optical devices, an iris diaphragm is set at the focal position of the first lens of the pair. The light through the lenses is attenuated by a neutral density filter (ND filter) and a slit, and is detected by a microchannel-plate type photomultiplier tube (MCP-PMT, Hamamatsu Photonics, R3809U-52), which has an excellent time resolution (rise time of 0.15 ns, transit time spread of 25 ps). The output signals of the MCP-PMT are processed by a constant fraction discriminator (CFD, TENNELEC, TC454) and are used as the start signal of the time-to-amplitude converter (TAC, ORTEC 467). On the other hand, a stop signal which is synchronized with the trigger signal of the pulser is used by the TAC. The output signals of the TAC are amplified and analyzed with a multichannel analyzer (MCA, Laboratory Equipment).

The time structure of the shutter is shown in Fig. 8. The ordinate and the abscissa in the figure correspond to the counting rate of the photons and the time, respectively. The full width of the shutter is about 2.0 ns and 1.0 ns in FWHM as seen in Fig. 8. An extinction ratio, which is defined as the ratio of the intensity of the singled-out light to that of the leaked light, of 800 is obtained. Because the bunch spacing of the PF-ring is 2 ns, it is possible to single out light from one particular bunch in the multi-bunch operation with the shutter system.

Experiment with SR in Multi-Bunch Operation

We installed the shutter system in beamline 21 (BL-21) in the PF-ring and tried to pick out a light pulse from a certain bunch in the multi-bunch operation. The shutter was triggered by a signal synchronized to the revolution of the bunches. In order to generate the trigger, the RF signal of the PF-ring was divided by 312, that is, a harmonic number. Figure 9 shows the time structure of the light passing through the shutter measured by the photon counting method. The three peaks in the figure show the count rates of the photons from 3 successive bunches. The count rate of the central peak, which corresponds to the picked-out bunch, is about 300 times as large as those of the others although the electron number in each bunch is almost equal; that is, a shutter system which has an extinction ratio of 300 is obtained for SR. This shows that the shutter works properly by picking out a particular bunch in the bunch train in the multi-bunch operation.

In the experiment with the CW-laser, the extinction ratio was 800. This figure is about 3 times larger than the ratio for SR. The reason is that the rotation of the polarization in the cell depends on the wavelength of the incident light; therefore, it is difficult to single out the SR as clearly as monochromatic light, like laser light, because the SR has a wide wavelength range. Details are given in Appendix C.

3.2 Detection of Betatron Oscillation of Individual Bunches with Optical Method

In order to detect betatron oscillation of individual bunches in the bunch train, we have developed an optical betatron oscillation detection system

which is composed of the high-speed light shutter and an optical betatron oscillation detector. A block diagram and the optical setup of the system are shown in Fig. 10. The image of the beam is focused by a lens system set behind the shutter. Because half of the image is cut off by a horizontal edge, the intensity of the light through the edge varies in response to the vertical motion of the beam. We use a photomultiplier tube (PMT, Hamamatsu Photonics, H2431-50) to measure the intensity. The change in amplitude of the signal selected by the shutter is analyzed with a spectrum analyzer (ADVANTEST, R3361D).

Because the light shutter has an extinction ratio of 300 at the most, the contribution of leaked light pulses through the shutter during the closing time is not negligible. The spectral lines corresponding to the betatron oscillations of all bunches appear as sidebands of the harmonics of the revolution frequency. Meanwhile, those corresponding to the singled-out bunch appear on both sides of the harmonics of the shutter frequency. Therefore, we can distinguish the betatron oscillation of the selected bunch from the contributions of the other bunches by detecting the betatron sidebands (f_{obs}) of the spectral lines that are not harmonics of the revolution frequency (f_{rev}) but of the shutter frequency ($f_{shutter} = \frac{1}{3}f_{rev}$), i.e.,

$$f_{obs} = \frac{n}{3}f_{rev} \pm qf_{rev} \quad \left(\frac{n}{3} \neq \text{integer} \right), \quad (3.1)$$

where q is the decimal part of the vertical tune (0.28).

As described in previous sections, the optical detection system is free from ringing and less affected by electromagnetic noise. On the other hand, the system is weak in quantitative detection of the betatron oscillation amplitude because the system uses the edge to detect the oscillation of the light.

Chapter 4

Results

4.1 Change in Tunes

4.1.1 Measurement and Analysis of Tunes

Betatron oscillations of all bunches due to the instability are detected independently in several multi-bunch conditions shown in Table 4.1. In order to make the observation of the instability clear, we turned off the octupole magnets to avoid the Landau damping effect during the experiments. Therefore, the amplitude-dependent tune shift due to non-linear magnetic fields is negligible. The initial bunch current was set to be 1.6 mA/bunch in all experiments. Figures 11 and 12 show spectra which correspond to the betatron sidebands of the 1st and 20th bunch in the 280-bunch train (Exp.1), respectively. Although the beam currents of these two bunches were almost the same, not only the spectral powers but also the frequencies are different, as seen in the figures.

In order to determine the tunes, we calculated the first-order moments of the spectra. Figures 13 - 15 show measured tune shifts from the tune of

Table 4.1: Experimental conditions.

Experiments	Number of Bunches	Empty Buckets	Change in Tune $\left(\frac{\Delta\nu_x}{\Delta n}\right) [\times 10^{-6}/\text{bunch}]$
Exp.1	280	32	4.0
Exp.2	100	212	2.1
Exp.3	50	262	1.7

(The bunch current is 1.6 mA/bunch in all experiments.)

the first bunch as a function of the bunch position in the train. When the train length is long (280 bunches), it is clearly seen that the tunes gradually increase along the train in the head and decrease again in the tail as seen in Fig. 13 despite a relatively large error in the tune measurements of around $\pm 0.5 \times 10^{-4}$ which is almost the same as the width of scattering of the tunes in the middle of the train.

4.1.2 Correction of Dependence of Tunes on Beam Current

Because the beam current varies during the measurement and the tune shift depends on the beam current,¹ it is necessary to correct for this dependency. In order to obtain data for the correction, we measured the dependence of the tune on the beam current in a single-bunch operation, in which the ion-trapping effect does not occur.

Figure 16 shows the experimental result of the dependence of the tune on the beam current. We fitted the data with a 3rd-order polynomial curve, and the coefficients of the polynomial are shown in Table 4.2. As seen in the table, the measured current dependence of the tune is about $-1.2 \times 10^{-4}/\text{mA}$.

¹The dependence of the tunes on the beam current is discussed in Appendix D.

Table 4.2: Dependence of the tune on the beam current.

Coefficient	Value
P_0	4.28
P_1	-1.18×10^{-4}
P_2	6.52×10^{-7}
P_3	-7.73×10^{-10}
Polynomial = $\sum_{n=0}^3 P_n I^n [\text{mA}]$	

Table 4.3: Decrease of the bunch current in the experiments.

Experiments	Number of Bunches	Decrease of Bunch Current [mA]
Exp.1	280	0.13
Exp.2	100	0.06
Exp.3	50	0.02

Typical decreases of the bunch current in the experiments are shown in Table 4.3. As seen in the table, the decreases of the bunch current are less than 10 % of the initial bunch current of 1.6 mA/bunch; therefore, the correction is not large compared with the measured tune shift. Furthermore, we controlled the bunch currents of individual bunches within 10% to avoid the current-dependence of the tune.

4.1.3 Change in Tunes in Head of Bunch Train

As described in Sec. 4.1.1, the tunes gradually increase along the bunch train in the head when the train length is long (280 bunches). The change in the vertical tunes $\left(\frac{\Delta\nu_y}{\Delta n}\right)$ along 20 successive bunches in the head of the train are evaluated with a linear fit, and shown in Table 4.1. The change in

the vertical tune along the bunch train caused by the FBII is estimated at $\frac{\Delta\nu_y}{\Delta n} = 1.8 \times 10^{-7}/\text{bunch}$ as discussed in Sec. 2.2 under the same conditions shown in Table 4.1. As seen in the table, the measured values for Exp.2 and Exp.3 are about 10 times and for Exp.1 about 40 times as large as the estimated value. The results seem to be related to the fact that the bunch gap with 262 empty buckets is not sufficient to clear ions completely; therefore, the electron beam is surrounded by ion-clouds under this condition.

4.2 Change in Amplitude

As seen in Figs. 11 and 12, the power spectrum changes along the bunch train. We estimated the peak power of the spectrum $P_{\beta y}$ by fitting the peak region of the spectrum with a polynomial curve. Because the peak power depends not only on the amplitude of the oscillation of the bunch but also on the bunch intensity, it is necessary to normalize the power with the intensity.

In order to measure the intensity under the tune-measurement we observed both the spectral component of $f_{shutter} + f_{\beta y}$ and a component of $f_{shutter}$ for individual bunches simultaneously. Because the power of the spectrum depends on the intensity of the selected bunch, we can estimate the intensity of the individual bunches by analyzing the peak power $P_{shutter}$ of the spectral component. After the estimation we normalize $P_{\beta y}$ with $P_{shutter}$ and determine $\sqrt{\frac{P_{\beta y}}{P_{shutter}}}$ as the amplitude.

Figures 17-19 show the amplitudes as a function of the bunch position in the train in Exp.1 - 3. The amplitude of the first bunch is defined as unity in each figure. The errors of the amplitude measurement are estimated at ± 0.4 in all experiments. The amplitudes rise in the head of the train, especially in Figs. 18 and 19.

Chapter 5

Discussion

5.1 Change in Tunes

5.1.1 Long Bunch Train

Estimation of Neutralization Factor

It is necessary to determine the neutralization factor η to discuss the change in tunes. In order to obtain the value of η experimentally, we measured the vertical tunes in different total beam currents for the same configuration of the bunch train as in Exp.1.

A measured vertical tune ν_y^{exp} can be written as

$$\nu_y^{exp} = \nu_y^0 + \Delta\nu_y^{I_b} + \Delta\nu_y^{ion}, \quad (5.1)$$

where ν_y^0 the vertical tune determined by the magnet system, $\Delta\nu_y^{I_b}$ the tune shift due to the dependence of the tunes on the beam current discussed in Sec. 4.1.2, and $\Delta\nu_y^{ion}$ the tune shift due to the ion trapping discussed in Eq. (2.11). Therefore, the difference of the tunes $\Delta\nu_y^{exp}$ in different beam

currents for the same configuration of the bunch train can be written as

$$\Delta\nu_y^{exp} = (\Delta\nu_{y1}^{I_b} - \Delta\nu_{y2}^{I_b}) + (\Delta\nu_{y1}^{ion} - \Delta\nu_{y2}^{ion}), \quad (5.2)$$

where suffix 1 and 2 represent values in different beam currents.

The terms $\Delta\nu_{y1,2}^{I_b}$ are already known from the correction data as discussed in Sec. 4.1.2 and Fig. 16; therefore, the difference of the tunes due to the change of the trapping condition of the ions can be written as

$$(\Delta\nu_{y1}^{ion} - \Delta\nu_{y2}^{ion}) = \Delta\nu_y^{exp} - (\Delta\nu_{y1}^{I_b} - \Delta\nu_{y2}^{I_b}). \quad (5.3)$$

Now we assume that the neutralization factor η does not change in the different beam currents. We rewrite Eq. (5.3) using Eq. (2.11):

$$(\Delta\nu_{y1}^{ion} - \Delta\nu_{y2}^{ion}) = \frac{r_e E_0}{2\pi E} \eta \left(\int_{C_1} \frac{\lambda_{e1} \beta_y}{\sigma_y (\sigma_x + \sigma_y)} ds - \int_{C_2} \frac{\lambda_{e2} \beta_y}{\sigma_y (\sigma_x + \sigma_y)} ds \right), \quad (5.4)$$

where $\lambda_{e1,2}$ are the averaged line densities of the electrons in each beam current. The integrals in Eq. (5.4) are taken over the regions $C_{1,2}$ where the ions are stably trapped around the beam in each beam current.

We measured the vertical tunes in different beam currents (total beam currents of 416.0 mA and 377.3 mA) for the same configuration of the bunch train (280 bunches + 32 empty buckets). After the correction of the dependence of the tunes on the beam current, we estimated the difference of the tunes. The difference is estimated at $+8.7 \times 10^{-5} \pm 8.2 \times 10^{-5}$.

Using the difference of the tunes, we estimated the neutralization factor from Eq. (5.4). The integrals in Eq. (5.4) are estimated numerically by calculating the area where the ions are stably trapped under the beam condition and taking the integrals over the area. An ion species of CO^+ is assumed again in the calculation. The neutralization factor is estimated at $7.5 \times 10^{-5} \pm 6.9 \times 10^{-5}$ for the configuration of the bunch train although the

accuracy of the measurement is not sufficient because the current dependence of the tunes is small.

Estimation of Theoretical Value

We calculated the theoretical values of the tune shifts along the train taking into account the modulation of ion density using Eq. (2.12). Figure 20 shows the experimental and the theoretical values of the tune shifts of all bunches corresponding to Exp.1 (280-bunch train). In the calculation of the theoretical values, an ion species of CO^+ and a neutralization factor η of 9.4×10^{-6} , which is consistent with the experimental value, are assumed.

In the calculated tune shift in Fig. 20, an asymmetry around the center of the bunch train can be seen although the “ion betatron function” β_i is symmetric, as mentioned in Sec. 2.1.2. This is because the asymmetry arises from the change in the beam current during the measurement. The pattern of the calculated tune shift wiggles in unison with the modulation of the ion density due to the oscillation of the ions, as seen in Fig. 20. Although the amplitude and periods of the wiggles in the middle part of the bunch train are averaged out by the averaging in Eq. (2.13), the pattern characteristically rapidly rises in the head of the train and falls in the tail. This characteristic is also clearly seen in the experimental results, as seen in Fig. 20. The increase of the tunes in the head of the bunch train is always observed in a series of experiments with the long bunch train. To further quantify the phenomenon, we calculated the averaged tune shifts along 20 bunches in the head. A theoretical value of $\left(\frac{\Delta\nu_y}{\Delta n}\right) = 5.1 \times 10^{-6}/\text{bunch}$ was obtained, which agree closely with the experimental value is shown in Table 4.1. On the other hand, the averaged tune shifts along 20 bunches in the tail is $\left(\frac{\Delta\nu_y}{\Delta n}\right) = -2.1 \times 10^{-6}/\text{bunch}$ from the experiments and -6.4×10^{-6} from the

theory. The agreement is not as good as in the head; however, a decrease of the tunes in the tail of the train is observed.

The wiggle pattern seen in the calculation reappears in the measurement, although the peaks and valleys of the patterns do not coincide with each other in the middle part of the train. The wiggle pattern of $\epsilon_y(\tau)$ in the middle part of the bunch train is smeared in the averaging of $1/\sqrt{\beta_i}$ given in Eq. (2.13); however, the pattern of the tune shifts in the head and the tail remains in the averaging because the ion betatron function at any location in the ring has a tendency to decrease along the bunch train head and increase along the tail. This is one of the reasons why the tune shift pattern in the middle part of the train is vague but has a clear increase in the head and a decrease in the tail.

5.1.2 Short Bunch Trains

For short bunch trains (Exp.2,3), the variations of the tune shifts were small compared with the case for the long train (Exp.1). According to the classical theory of ion-trapping, ions like CO^+ cannot be trapped around the beam if the number of the bunches in the train is less than 100 in the PF-ring, as seen in Fig. 2. The experimental values are roughly 10 times as large as that predicted by the FBII theory.

We performed a simulation of the ion motion for the short bunch trains and calculated the change in the vertical tunes. In the simulation, we adopted both an ion-creation effect and a modulation of the ion density, and treated the electric field induced by a bunch as a non-linear field[13] in contrast with the discussion in Sec. 2.1.1. The result was almost equal to the theoretical value from the FBII theory but does not correspond to the experimental value.

To resolve the disagreement, we are planning to measure the number of trapped ions by detecting bremsstrahlung gamma rays emitted by scattering between the electron and the residual gas molecules or the ions. Construction of a theory which can be used for a transient ion trapping phenomenon is also a future subject.

5.2 Change in Amplitudes

As seen in Figs. 17-19, the oscillation amplitudes of the individual bunches depend on their positions in the train, and, in particular, the amplitudes rise in the head of the train.

Because we use the edge to detect the oscillation of the light in the optical beam diagnostic system as shown in Fig. 10, it is difficult to measure the amplitude when that the amplitude is larger than the spot size on the edge, as discussed in Sec. 3.2. The data of the amplitudes in Figs. 17-19 have such a “saturation” problem; therefore, quantitative discussion of the dependence of the amplitudes on the position in the train is difficult at present. Moreover, we built the detector on a beamline for a photon counting system that requires merely weak light; therefore, the intensity of light provided by the beamline is insufficient for the beam diagnostics in our present experiment and the S/N ratio of the measurement is unsatisfactory. Improvement of the beamline and further development of an optical beam diagnostic system that is better able to detect the oscillation amplitude quantitatively are future subjects. Now we plan to develop a new detection system using a fast-response position sensitive detector ¹ and to improve the beamline.

¹For example, we are planning to use a 2-dimensional position sensitive detector (S2044, Hamamatsu Photonics) which has a good time response (rise time of 0.3 μ s) and good spatial resolution (0.6 μ m).

Chapter 6

Conclusion

In order to observe the beam instability in the PF-ring, we have developed a bunch-by-bunch beam diagnostic system which can detect the betatron tunes of individual bunches in a multi-bunch condition. The system is composed of a high-speed light shutter and an optical beam oscillation detector. The light shutter, which is composed of a pockels cell and polarizers, can be opened or closed within 2 ns. Light through the shutter is focused on a horizontal edge and detected by a PMT. The vertical motion of the beam can be detected as an amplitude variation of the output signal of the PMT because the intensity of the light through the edge varies in response to the movement of the image of the beam on the edge. Because the light shutter has an extinction ratio of 300 at the most, the contribution of leaked light pulses through the shutter during the close timing is not negligible. However, we can distinguish betatron oscillation of the selected bunch from the oscillations of the other bunches by setting the repetition rate of the shutter to be $\frac{1}{3}f_{rev}$ and by detecting betatron sidebands of frequencies that are not revolution harmonics but shutter-frequency harmonics.

In the experiments of the long bunch train (280 bunches), vertical tunes

rise in the head and fall in the tail of the train. In order to explain this phenomenon, we discussed the motion of trapped ions with a method similar to the theory of betatron oscillations in circular accelerators. From the discussion, we considered a theoretical model in which the density of the ions are modulated along the bunch train and tune shifts that depend on position in the train occur. We calculated the change in the vertical tunes along the train and compared the theoretical values with the experimental results.

We fitted the theoretical values to the experimental results by optimizing a neutralization factor η . In order to estimate η independently, we measured the dependence of the tune on the total beam current while keeping the pattern of the bunch train unchanged. The estimated η is consistent with the fitted value. We calculated the averaged tune shifts along 20 bunches in the head. The agreement between the theoretical value and the experimental value was fairly good. On the other hand, the agreement in the tail was not as good as in the head; however, the decrease of the tunes predicted in the theory was observed.

We also analyzed the oscillation amplitudes of individual bunches using the power spectra of the betatron sidebands. It is difficult to measure the amplitudes quantitatively because of saturation in the detector; however, we were able to show qualitatively that the amplitudes vary with position in the train. A more quantitative measurement of the amplitudes for individual bunches is a future goal.

In the experiments with short bunch trains, the vertical tunes rise in the head of the train. According to the classical ion-trapping theory, it is predicted that ions are rarely trapped. We compared the experimental results with the predictions from the FBII theory; however, they did not agree with each other. Construction of another transient ion-trapping theory and a

direct measurement of trapped ions are also future goals.

Appendix A

Ion Trapping

An electron beam circulating in a vacuum system of a storage ring collides with residual gas molecules and creates positive ions. They are attracted by an electric field induced by the beam and form ion-clouds around the beam orbit. The ions are affected by periodic focusing forces corresponding to the configuration of the bunch train and oscillate stably around the beam orbit if a stability condition discussed below is satisfied. On the other hand, the electron beam is also affected by focusing forces caused by the electric field induced by the ion-clouds, and accordingly, a tune shift occurs.

In this chapter, we summarize the motion of the trapped ions and the effect of the trapped ions on the beam motion.

A.1 Ion Motion

We consider the motion of an ion which has a positive charge $+e$ and a mass number of A . When a bunch passes near the ion, the ion is affected by the attractive force of the beam. Because the bunch is short (about 50 ps), the attractive force can be treated as a single kick, i.e., a delta function.

We assume the bunch has a 2-dimensional gaussian charge distribution in the (x, y) plane and is short along the z axis:

$$\rho = -\frac{e\lambda_e(z)}{2\pi\sigma_x\sigma_y} \exp\left(-\frac{x^2}{2\sigma_x^2} - \frac{y^2}{2\sigma_y^2}\right), \quad (\text{A.1})$$

where $\sigma_{x,y}$ are horizontal/vertical beam sizes and $\lambda_e(z)$ is the averaged line density of the electron given by

$$\lambda_e(z) = N_b\delta(z), \quad (\text{A.2})$$

where N_b is the number of the electrons per bunch.

The electric fields $\mathcal{E}_{x,y}^{beam}$ induced by the bunch (A.2) can be written analytically in a linear approximation [17]:

$$\left. \begin{aligned} \mathcal{E}_x^{beam} &= -\frac{e\lambda_e(z)}{2\pi\epsilon_0\sigma_x(\sigma_x+\sigma_y)}x \\ \mathcal{E}_y^{beam} &= -\frac{e\lambda_e(z)}{2\pi\epsilon_0\sigma_y(\sigma_x+\sigma_y)}y \end{aligned} \right\} \quad (\text{A.3})$$

In the following sections, we only consider the vertical component of the electric fields in (A.3) because the vertical beam size is much smaller than the horizontal size and effects on the ion motion due to the horizontal component of the electric field are negligible.

The equation of motion of the ion is written as

$$Am_p \frac{d^2 y_i}{dt^2} = -\frac{e^2 \lambda_e(z)}{2\pi\epsilon_0\sigma_y(\sigma_x+\sigma_y)} y_i, \quad (\text{A.4})$$

where m_p is the mass of a proton. Eq. (A.4) can be integrated giving

$$\left. \begin{aligned} \dot{y}_{i,1} &= -\frac{2r_p c N_b}{A\sigma_y(\sigma_x+\sigma_y)} y_{i,0} + \dot{y}_{i,0} \\ y_{i,1} &= y_{i,0} \end{aligned} \right\}, \quad (\text{A.5})$$

where \dot{y}_i is the vertical velocity of the ion and the suffixes 0 and 1 represent the values before and after the passage of the bunch. Eqs. (A.5) can be

written in simple matrix form:

$$\begin{pmatrix} y_i \\ \dot{y}_i \end{pmatrix}_1 = \begin{pmatrix} 1 & 0 \\ a & 1 \end{pmatrix} \begin{pmatrix} y_i \\ \dot{y}_i \end{pmatrix}_0, \quad (\text{A.6})$$

$$a = -\frac{2r_p c N_b}{A\sigma_y(\sigma_x + \sigma_y)}. \quad (\text{A.7})$$

After the passage of the bunch, the ion drifts freely until the next bunch comes. The complete matrix of the passage of the bunch is written as a product of the single kick and the drift motion matrices:

$$\begin{pmatrix} y_i \\ \dot{y}_i \end{pmatrix}_1 = \begin{pmatrix} 1 & t_{rf} \\ 0 & 1 \end{pmatrix} \begin{pmatrix} 1 & 0 \\ a & 1 \end{pmatrix} \begin{pmatrix} y_i \\ \dot{y}_i \end{pmatrix}_0. \quad (\text{A.8})$$

Eq. (A.8) corresponds to Eq. (2.2) in Sec. 2.1.1.

A.2 Tune Shift

The ions attracted by the beam induce an electric field which affects the beam as a focusing force, and accordingly, a tune shift occurs.

We assume that the ion cloud has a 2-dimensional gaussian charge distribution in the (x, y) plane and a uniform distribution along the s axis:

$$\rho_{ion} = \frac{e\lambda_i}{2\pi\Sigma_x\Sigma_y} \exp\left(-\frac{x^2}{2\Sigma_x^2} - \frac{y^2}{2\Sigma_y^2}\right), \quad (\text{A.9})$$

where λ_i is the averaged line density of the ion and $\Sigma_{x,y}$ are horizontal and vertical sizes of the ion cloud, respectively. The line density λ can be written as the product of the averaged line density of the electrons and a neutralization factor:

$$\begin{aligned} \lambda_i &= \eta \frac{I_{tot}}{ec} \\ &= \eta \lambda_e, \end{aligned} \quad (\text{A.10})$$

where I_{tot} is the total beam current.

The electric fields \mathcal{E}_x and \mathcal{E}_y induced by the ion cloud (A.9) can be written analytically in a linear approximation [17]:

$$\left. \begin{aligned} \mathcal{E}_x &= \frac{e\eta\lambda_e}{2\pi\epsilon_0\Sigma_x(\Sigma_x+\Sigma_y)}x \\ \mathcal{E}_y &= \frac{e\eta\lambda_e}{2\pi\epsilon_0\Sigma_y(\Sigma_x+\Sigma_y)}y \end{aligned} \right\} \quad (\text{A.11})$$

In the following discussion, we only consider the vertical component of the electric field because of reasons similar to those discussed in App. A.1.

The tune shift $\Delta\nu_y$ due to the focusing field (A.11) is written as:

$$\begin{aligned} \Delta\nu_y &= \frac{1}{4\pi} \int_C \frac{e}{E} \frac{\partial \mathcal{E}_y}{\partial y} \beta_y(s) ds \\ &= \frac{r_e E_0}{2\pi E} \lambda_e \eta \int_C \frac{\beta_y(s)}{\Sigma_y (\Sigma_x + \Sigma_y)} ds, \end{aligned} \quad (\text{A.12})$$

where the integral is over the area C where the ions are stably trapped, $\beta_y(s)$ is the vertical betatron function of the beam, r_e the classical electron radius, E_0 the rest mass of the electron and E the total energy of the electron.

Appendix B

Twiss Parameters

An electron in a storage ring is affected by a periodic force due to magnetic fields and oscillates around a closed orbit. In accelerator physics, the motion of the particle is written with parameters called Twiss parameters. In this chapter, we simply summarize the derivation of Twiss parameters and the motion of the particle with the parameters. Detailed discussions are in Reference [6].

B.1 Definition of Twiss Parameters

The equation of motion of a charged particle in a storage ring is given by Hill's equation:

$$\left. \begin{aligned} \frac{d^2 y(s)}{ds^2} + K(s)y(s) &= 0, \\ K(s) &= K(s + C_0) \end{aligned} \right\}, \quad (\text{B.1})$$

where C_0 is the circumference of the ring and $K(s)$ represents the periodic focusing force due to the magnets around the ring. The solution to Eq. (B.1)

is written in a matrix form as

$$\begin{pmatrix} y(s + C_0) \\ y'(s + C_0) \end{pmatrix} = \mathcal{M}(s) \begin{pmatrix} y(s) \\ y'(s) \end{pmatrix}, \quad (\text{B.2})$$

where a prime denotes differentiation with respect to s and $\mathcal{M}(s)$ is a matrix which represents the motion of the particle during one revolution around the ring.

The matrix $\mathcal{M}(s)$ has eigenvalues $\lambda_{1,2} = e^{\pm i\mu}$ because the determinant of $\mathcal{M}(s)$ is unity. Stability of the particle motion requires that μ is a real number satisfying

$$|\cos \mu| = \frac{1}{2} |\text{Tr } \mathcal{M}(s)| \leq 1. \quad (\text{B.3})$$

The matrix $\mathcal{M}(s)$ may be written with μ and other parameters $(\beta(s), \alpha(s), \gamma(s))$ as

$$\left. \begin{aligned} \mathcal{M} &= \mathcal{I} \cos \mu + \mathcal{J} \sin \mu, \\ \mathcal{I} &= \begin{pmatrix} 1 & 0 \\ 0 & 1 \end{pmatrix}, \quad \mathcal{J} = \begin{pmatrix} \alpha(s) & \beta(s) \\ -\gamma(s) & -\alpha(s) \end{pmatrix} \end{aligned} \right\}. \quad (\text{B.4})$$

The parameters $(\beta(s), \alpha(s), \gamma(s))$ are called the Twiss parameters, and need to satisfy the following relation because the determinant of $\mathcal{M}(s)$ is unity:

$$\gamma(s) = \frac{1 + \alpha^2(s)}{\beta(s)}. \quad (\text{B.5})$$

B.2 Particle Motion with Twiss Parameters

We consider eigenvectors which have eigenvalues $e^{\pm i\mu}$. According to Floquet's theorem, the first components $y_{1,2}(s)$ of the eigenvectors are given by

$$y_{1,2}(s) = b_0 \omega(s) e^{\pm i\psi(s)}, \quad (\text{B.6})$$

where b_0 is a constant and $\omega(s), \psi(s)$ are functions which satisfy

$$\left. \begin{aligned} \omega(s + C_0) &= \omega(s), \\ \psi(s + C_0) &= \psi(s) + \mu + 2\pi n \end{aligned} \right\}, \quad (\text{B.7})$$

where n is an integer. From Eqs. (B.1) and (B.6) we obtain

$$\left. \begin{aligned} \omega''(s) + K(s)\omega(s) - (\psi'(s))^2 \omega(s) &= 0, \\ \psi''(s)\omega(s) + 2\psi'(s)\omega'(s) &= 0 \end{aligned} \right\}. \quad (\text{B.8})$$

Next, we consider the motion of a particle at a position s . The motion $(Y(s), Y'(s))$ is written as a linear combination of $y_{1,2}(s)$ and $y'_{1,2}(s)$:

$$\begin{aligned} \begin{pmatrix} Y(s) \\ Y'(s) \end{pmatrix} &= \begin{pmatrix} y_1(s) & y_2(s) \\ y'_1(s) & y'_2(s) \end{pmatrix} \begin{pmatrix} a \\ b \end{pmatrix} \\ &= \mathcal{Y}(s) \begin{pmatrix} a \\ b \end{pmatrix}, \end{aligned} \quad (\text{B.9})$$

where a and b are constants. Similarly, the motion of the particle after one revolution around the ring is written as

$$\begin{pmatrix} Y(s + C_0) \\ Y'(s + C_0) \end{pmatrix} = \mathcal{Y}(s + C_0) \begin{pmatrix} a \\ b \end{pmatrix}. \quad (\text{B.10})$$

From Eqs. (B.9) and (B.10) we obtain

$$\begin{pmatrix} Y(s + C_0) \\ Y'(s + C_0) \end{pmatrix} = \mathcal{Y}(s + C_0) \mathcal{Y}^{-1}(s) \begin{pmatrix} Y(s) \\ Y'(s) \end{pmatrix}. \quad (\text{B.11})$$

From Eqs. (B.1), (B.4), (B.8) and (B.11) we obtain

$$\omega(s) = \sqrt{\beta(s)}, \quad (\text{B.12})$$

$$\beta'(s) = -2\alpha(s), \quad (\text{B.13})$$

$$\psi(s) = \int_0^s \frac{ds}{\beta(s)} + \psi_0, \quad (\text{B.14})$$

where ψ_0 is a constant. Using the Twiss parameters the particle motion is given by

$$\left. \begin{aligned} y(s) &= b_0 \sqrt{\beta(s)} \cos(\psi(s) + \psi_0), \\ y'(s) &= -b_0 \sqrt{\frac{1}{\beta(s)}} [\alpha(s) \cos(\psi(s) + \psi_0) + \sin(\psi(s) + \psi_0)] \end{aligned} \right\}. \quad (\text{B.15})$$

(B.15) is the expression of the betatron oscillation with the Twiss parameters.

Appendix C

High-Speed Light Shutter

A pockels cell is made of a KD_2PO_4 crystal and has a uniaxis of symmetry [16]. When a voltage parallel to the axis is applied to the cell, the refractive indices for two directions perpendicular to the direction of the electric field are different from each other. Therefore, the cell can be used as a phase-modulator and can rotate the polarization angle of light injected into the cell parallel to the axis of symmetry.

We define the direction of the incident light (parallel to the axis of symmetry) as z and the horizontal and vertical directions in the plane perpendicular to the z axis as x and y , respectively. We assume that the incident light has a horizontal polarization:

$$\left. \begin{aligned} E_x^{in} &= E_0 \sin(\omega t + \psi), \\ E_y^{in} &= 0, \end{aligned} \right\} \quad (\text{C.1})$$

where ω is the frequency of the incident light in rad/sec and ψ an initial phase.

The polarization angle of the light (C.1) rotates when a voltage is applied to the cell. The light which passes through the cell has not only a horizontal

but also a vertical component, namely,

$$\left. \begin{aligned} E_x^{out} &= E_0 \cos\left(\omega t - \frac{\omega n_0}{c} L - \frac{V}{V_H} \frac{\pi}{2} + \psi\right) \cos\left(\frac{V}{V_H} \frac{\pi}{2}\right) \\ E_y^{out} &= E_0 \cos\left(\omega t - \frac{\omega n_0}{c} L + \frac{V}{V_H} \frac{\pi}{2} + \psi\right) \sin\left(\frac{V}{V_H} \frac{\pi}{2}\right) \end{aligned} \right\}, \quad (\text{C.2})$$

where n_0 is the refraction index of the pockels cell when the voltage is not applied, L the length of the cell in the z direction, V the voltage applied to the cell and V_H the “half wavelength voltage” that gives a rotation angle of $\frac{\pi}{2}$. The half wavelength voltage depends on the wavelength of the incident light and physical characteristics of the cell:

$$V_H = \frac{\lambda}{2n_0^3 r_{63}}, \quad (\text{C.3})$$

where λ is the wavelength of the incident light and r_{63} a component of the electrooptic tensor [16]. The dependence of V_H on the wavelength is shown in Fig. 21 for the cell which we have used.

As described in Sec. 3.1.2, the extinction ratio differs for different light sources. One reason for the difference arises from the difference in coherence of the light source. A photodetector outputs signals whose magnitude varies linearly with the power of the transmission light of the shutter. We define the total number of photons which are transmitted through the shutter system as N . In the case of coherent light, as for a laser, the output signal V_{out} of the detector is

$$\begin{aligned} V_{out} &\propto (N \cos(\omega t + \psi))^2 \\ &\propto \sin^2\left(\frac{\pi}{2} \frac{V}{V_H}\right). \end{aligned} \quad (\text{C.4})$$

On the other hand, for incoherent light, like the SR which we have used, the output signal is proportional to the power of the light integrated over the phase:

$$V_{out} \propto \left(\sum_i^N \cos(\omega t + \psi_i) \right)^2$$

$$\begin{aligned}
& \propto \sum_i^N (\cos(\omega t + \psi_i))^2 + \sum_{i \neq j}^N \cos(\omega t + \psi_i) \cos(\omega t + \psi_j) \\
& \propto \sin\left(\frac{\pi}{2} \frac{V}{V_H}\right). \tag{C.5}
\end{aligned}$$

Therefore, the magnitude of the output signal depends not only on the intensity but also on the coherence of the light.

Another reason for the variation of the extinction ratio arises from the dependence of the half wavelength voltage on the wavelength. Because the SR light covers the wavelength region of visible light, the transmission rate depends on the spectral distribution of the SR. Therefore, it is difficult to pick out the SR as clearly as monochromatic light, as for a CW-laser.

Appendix D

Laslett Tune Shift

Tune shifts are caused not only by an ion-trapping effect but also by electromagnetic fields induced by the beam itself. The phenomenon induced by a space charge effect is called the Laslett tune shift [3].

We consider a bunched beam that has a longitudinal charge density $\hat{\lambda}e$ and moves with a speed of βc . Because the beam has a transverse charge distribution, an electric field and magnetic field are induced, and the beam is affected by the fields induced by the beam itself. This phenomenon is called a direct space charge effect, and causes tune shifts. Tune shifts are also induced by environmental conditions, such as the vacuum chamber and the magnet pole faces.

The vertical tune shift $\Delta\nu_y$ due to the space charge effect and the environmental conditions is obtained by calculating the Lorentz forces due to the electric and magnetic fields induced by the beam as

$$\Delta\nu_y = -\frac{r_e R^2}{\nu_{y0} \beta^2 \gamma} \left[\frac{1}{\gamma^2} \left(\frac{\pi^2}{24} \frac{1}{h^2} + \frac{1}{a^2} \right) \hat{\lambda} + \beta^2 \left(\frac{\pi^2}{12g^2} + \frac{\pi^2}{24h^2} \right) \bar{\lambda} \right], \quad (\text{D.1})$$

where r_e is the classical electron radius, R the averaged radius of the storage ring, ν_{y0} the original value of the vertical tune, γ the Lorentz factor of the

beam, h the half length of the vacuum chamber height, g the half length of the magnet gap height and a the transverse beam radius. $\hat{\lambda}$ and $\bar{\lambda}$ are the local charge density and the averaged charge density defined as

$$\hat{\lambda} = \frac{N_b}{\sqrt{2\pi}\sigma_z}, \quad (\text{D.2})$$

$$\bar{\lambda} = \frac{n_b N_b}{2\pi R}, \quad (\text{D.3})$$

where N_b is the number of the electrons in one bunch, σ_z the longitudinal bunch length and n_b the number of the bunches. Detailed derivation of Eq. (D.1) is in Reference [3].

Bibliography

- [1] R. D. Kohaupt,
“Mechanismus der Ionenabsaugung im Elektron-Positron-Speicherring (DORIS)”,
DESY, Interner Bericht No. H1-71/2, 1971.
- [2] Y. Baconnier, G. Brienti,
“The Stability of Ions in Bunched Beam Machines”,
CERN Internal Report No. CERN/SPS/80-2(DI), 1980.
- [3] A. W. Chao,
Physics of Collective Beam Instabilities in High Energy Accelerators,
(Wiley-Interscience Publication, New York, 1993).
- [4] Photon Factory Activity Report **15**,
edited by K. Haga *et al.*, 1997.
- [5] A. Mochihashi, T. Kasuga, T. Obina, M. Tobiyama,
“Bunch-by-Bunch Beam Diagnostics Using A Fast Light Shutter”,
in *Proceedings of the 1st Asian Particle Accelerator Conference, Tsukuba, 1998*, edited by Y. H. Chin *et al.*
(High Energy Accelerator Research Organization, 1998), p. 549.

- [6] H. Wiedemann,
Particle Accelerator Physics I,II,
(Springer-Verlag, Berlin, 1998).
- [7] T. O. Raubenheimer, F. Zimmermann,
“Fast Beam-Ion Instability. I. Linear Theory and Simulations”,
Phys. Rev. E **52**, 5487 (1995).
- [8] H. Kobayakawa, K. Huke, M. Izawa, Y. Kamiya, M. Kihara, M.
Kobayashi and S. Sakanaka,
“Observation of the Ion Trapping Phenomenon with Bremsstrahlung”,
Nucl. Instr. and Meth. A **248**, 565 (1986).
- [9] Y. Hori (private communication).
- [10] A. Mochihashi, T. Obina, Y. Tanimoto, T. Kasuga,
“Observation of Transverse Instability Using Bunch-by-Bunch Beam Di-
agnostic System in KEK-PF”,
in *Proceedings of the 7th European Particle Accelerator Conference, Vi-
enna, 2000*. (to be published)
- [11] T. Obina, T. Kasuga, M. Tobiyama, T. Katsura, K. Tamura,
“Measurement of the Longitudinal Bunch Structure in the Photon Fac-
tory Positron Storage Ring with a Photon Counting Method”,
Nucl. Instr. and Meth. A **354**, 204 (1995).
- [12] K. Tamura,
“The Longitudinal Wake Potential in the Vacuum Chamber Environ-
ment of the Photon Factory Electron Storage Ring”,
Doctoral thesis, Faculty of Science, Hiroshima University, 1997.

- [13] M. Bassetti, G. A. Erskine,
 “Closed Expression for the Electrical Field of a Two-Dimensional Gaussian Charge”,
 CERN Internal Report No. CERN-ISR-TH/80-06, 1980.

- [14] E. Keil, B. Zotter,
 “Landau-Damping of Coupled Electron Proton Oscillations”,
 CERN Internal Report No. CERN-ISR-TH/71-58, 1971.

- [15] R. A. Bosch,
 “The Trapped Ion-Electron Instability in an Electron Storage Ring with a Gap in the Bunch Train”,
 Nucl. Instr. and Meth. A **450**, 223 (2000).

- [16] G. Matone, A. Tranquilli,
 “Laser Light Modulation: The Electrooptic Effect” ,
 CNEN Internal Report No. LNF-76/7(R), 1976.

- [17] E. Keil,
 “Beam-Beam Interactions in p-p Storage Ring”,
 in *Theoretical Aspects of the Behaviour of Beams in Accelerators and Storage Rings*, edited by M. H. Blewett,
 CERN Report No. CERN 77-13, 1977, p. 314.

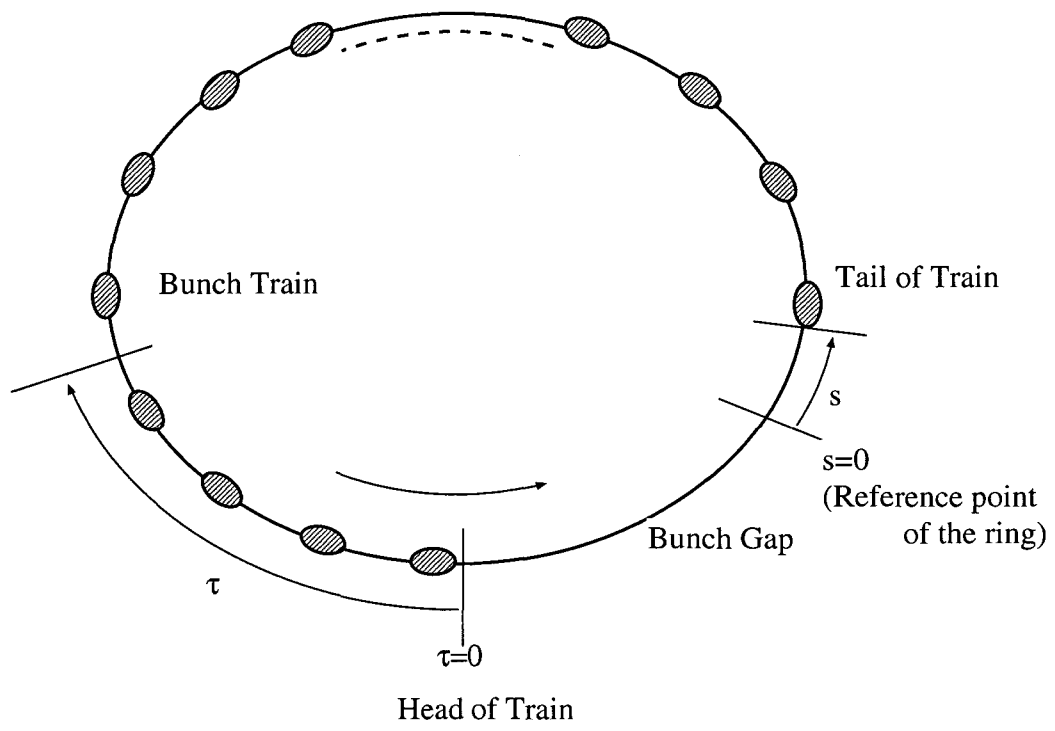


Figure 1: Definitions of parameters s and τ .

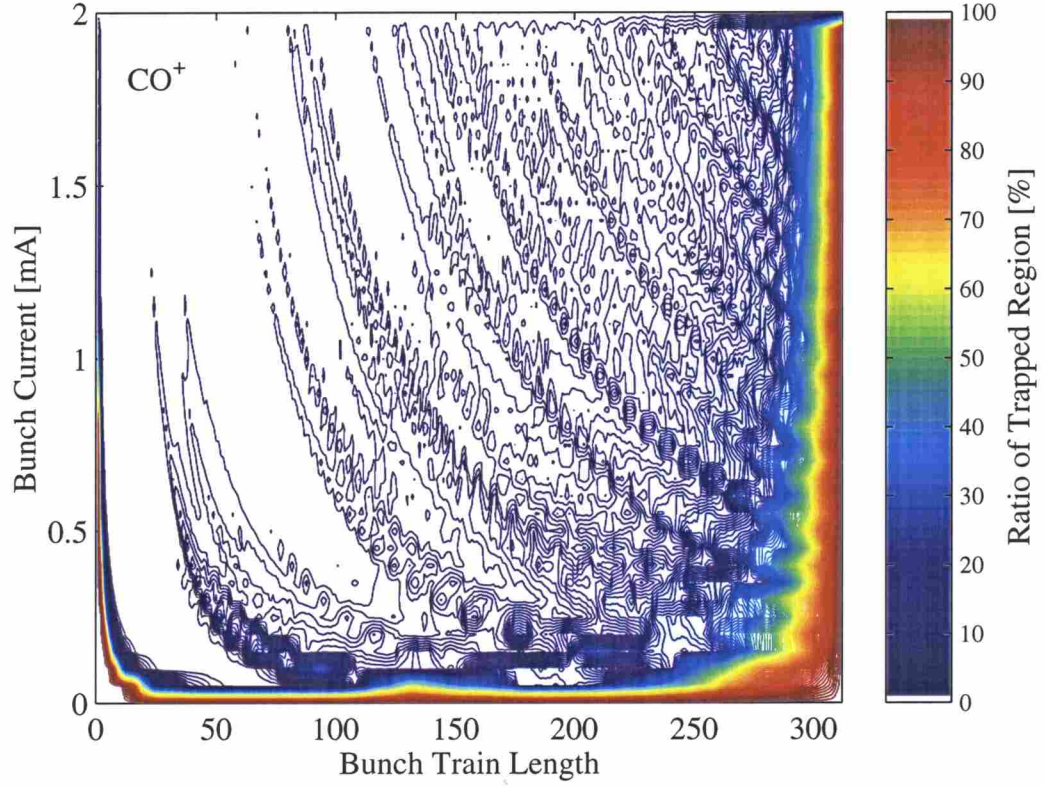


Figure 2: (Color) The ratio of the area of the regions where the ions are trapped to the area of the whole ring for various bunch train lengths. For example, the contour lines for 50% represent conditions in which the regions where the ions are trapped cover half of the whole ring.

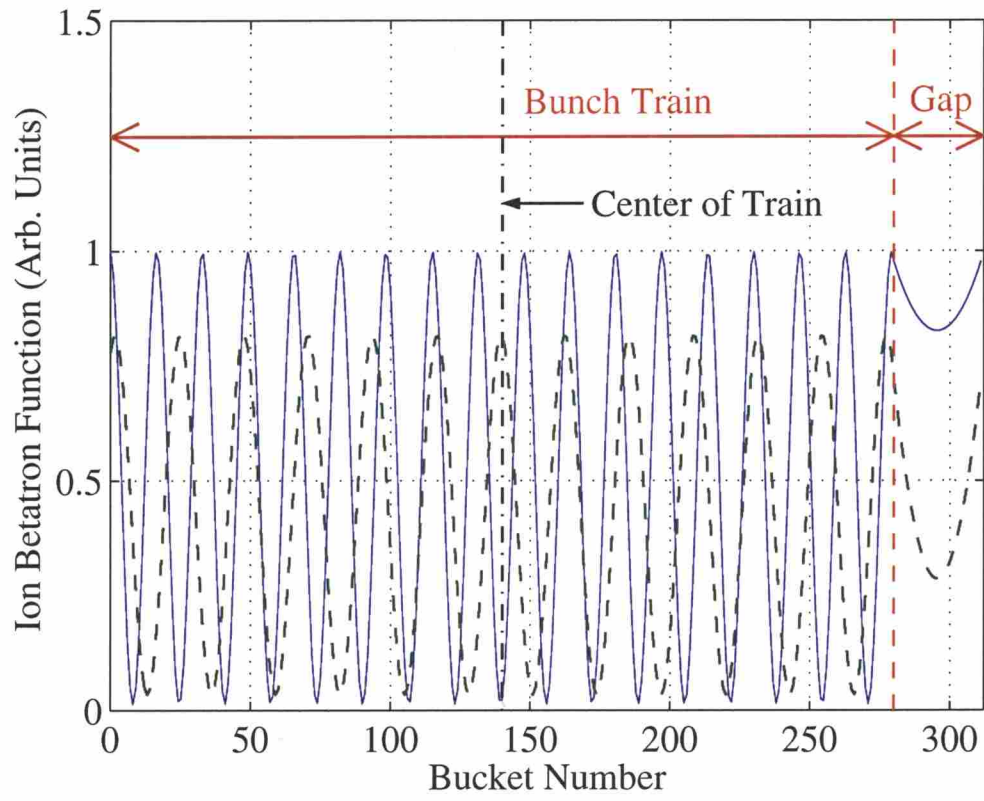


Figure 3: (Color) Ion betatron functions (solid-blue and dashed-green curves) at two different locations in the ring.

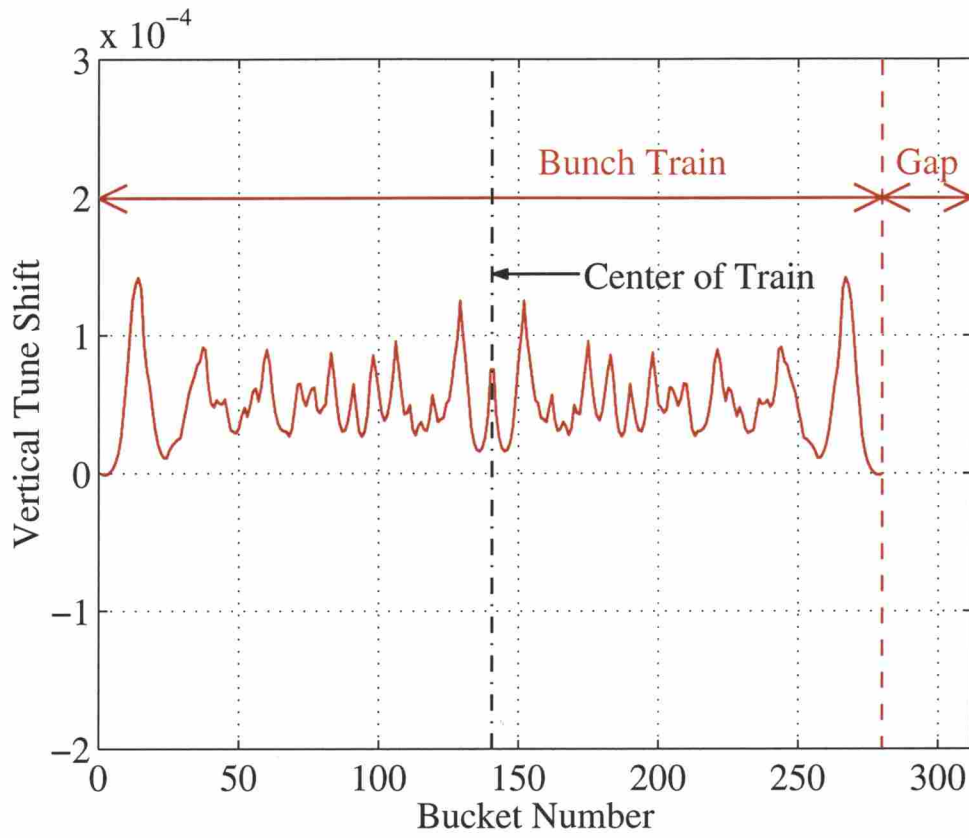


Figure 4: (Color) The theoretical calculation of the change in the tunes along a 280-bunch train.

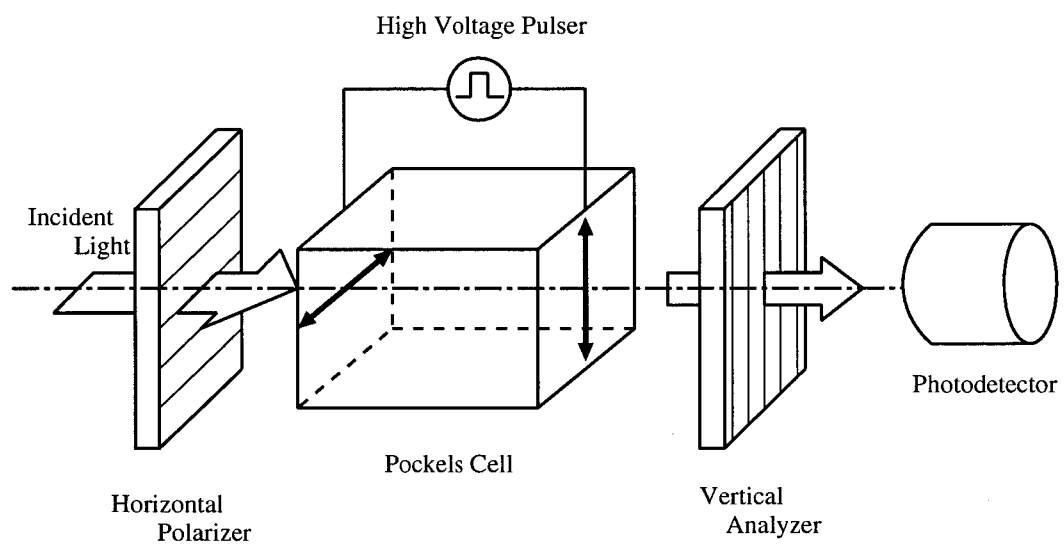


Figure 5: Schematic diagram of the high-speed light shutter.

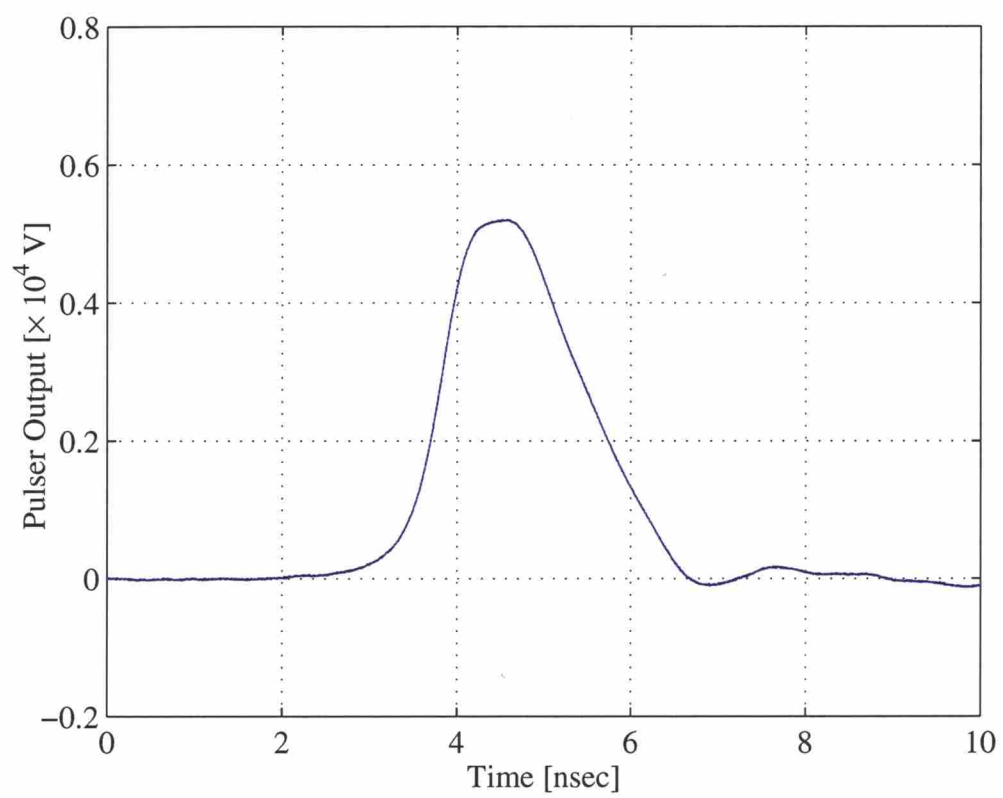


Figure 6: The output pulse of the high voltage pulser.

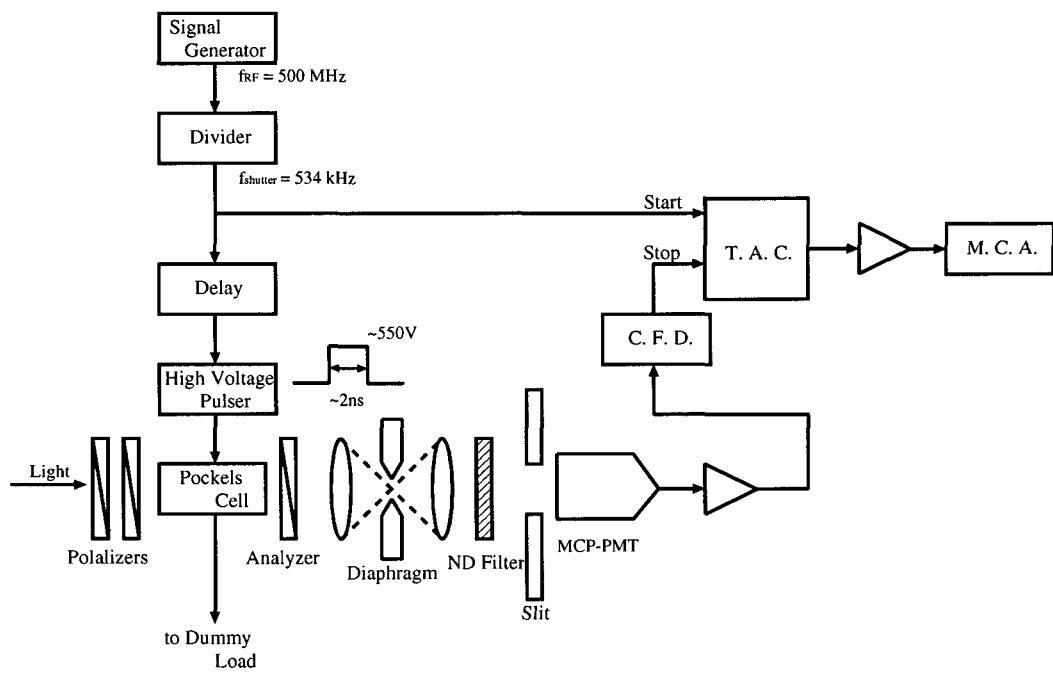


Figure 7: Block diagram, including the optical setup, of the high-speed light shutter.

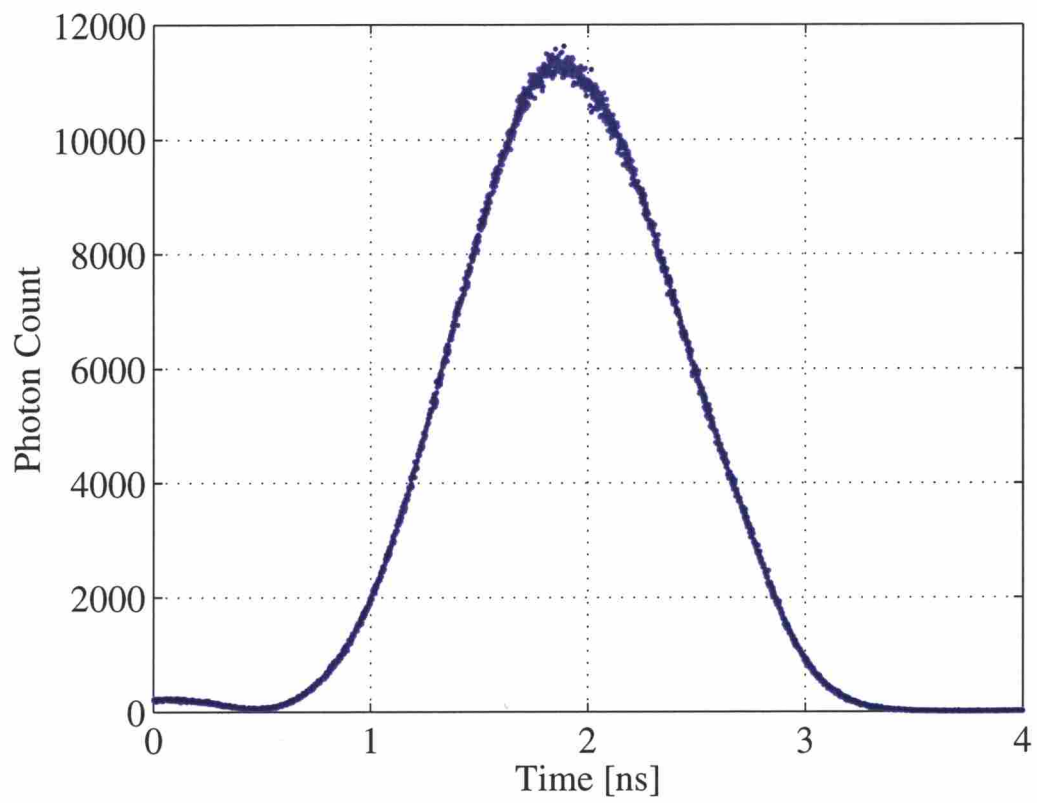


Figure 8: Time structure of the singled-out light pulse from the CW-laser.

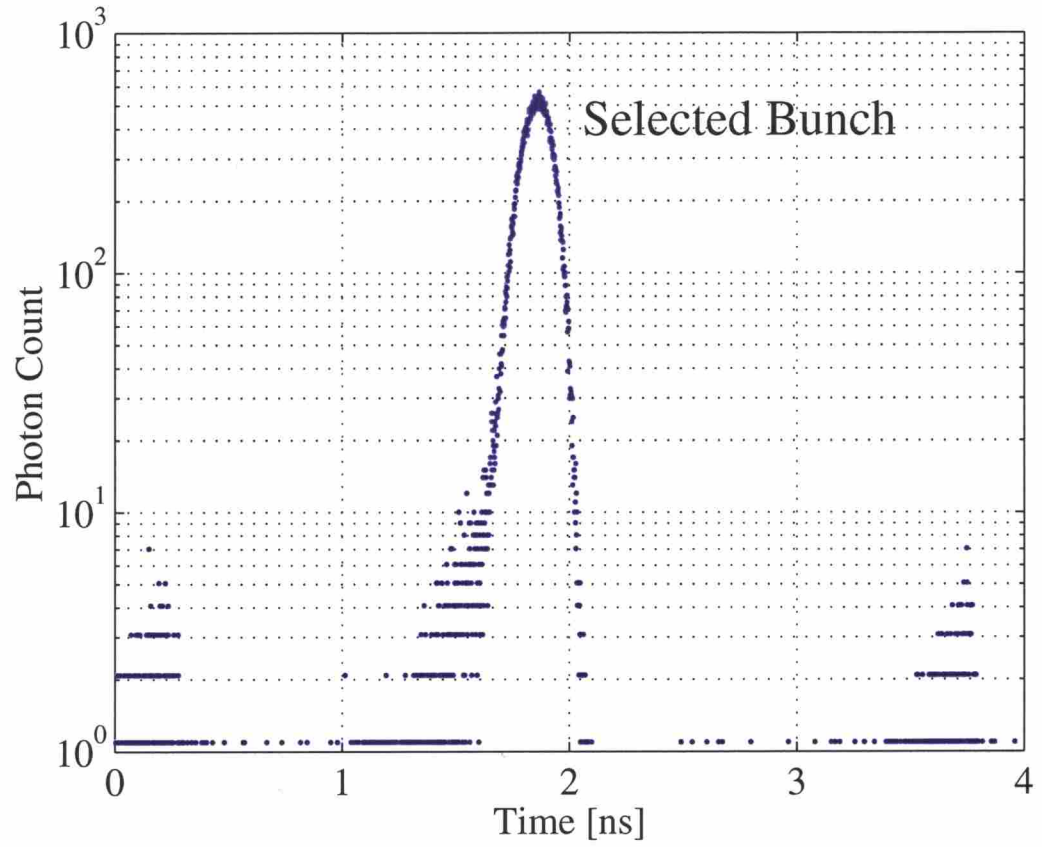


Figure 9: Time structure of the transmitted light. The SR of BL-21 in the PF ring at the multi-bunch mode was used as the light source.

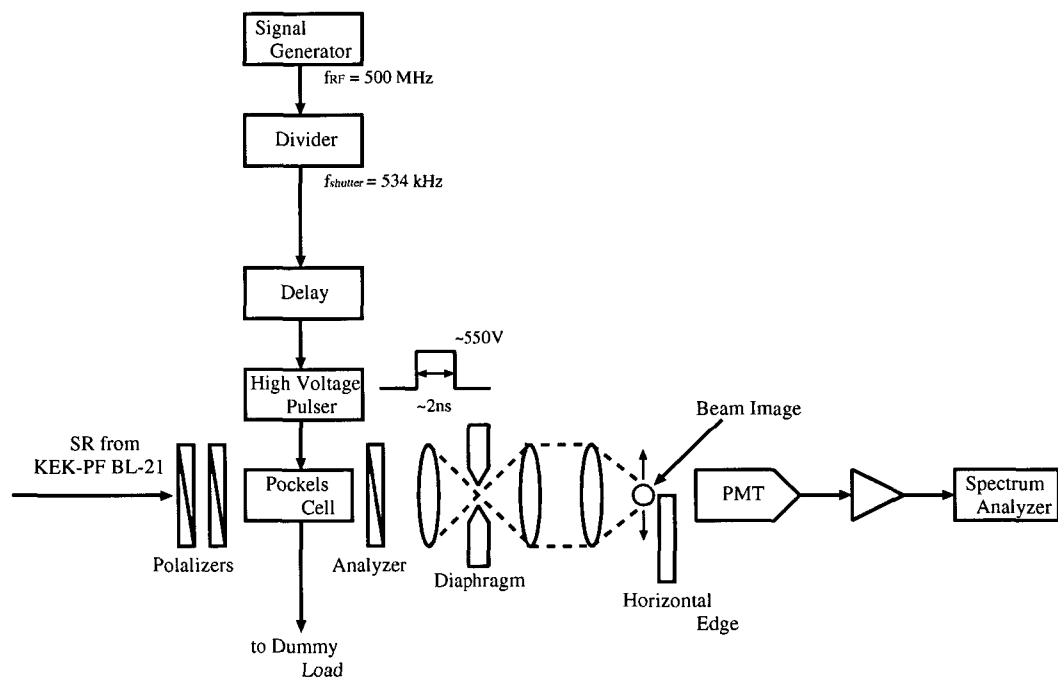


Figure 10: Block diagram and optical setup of the optical betatron oscillation detector.

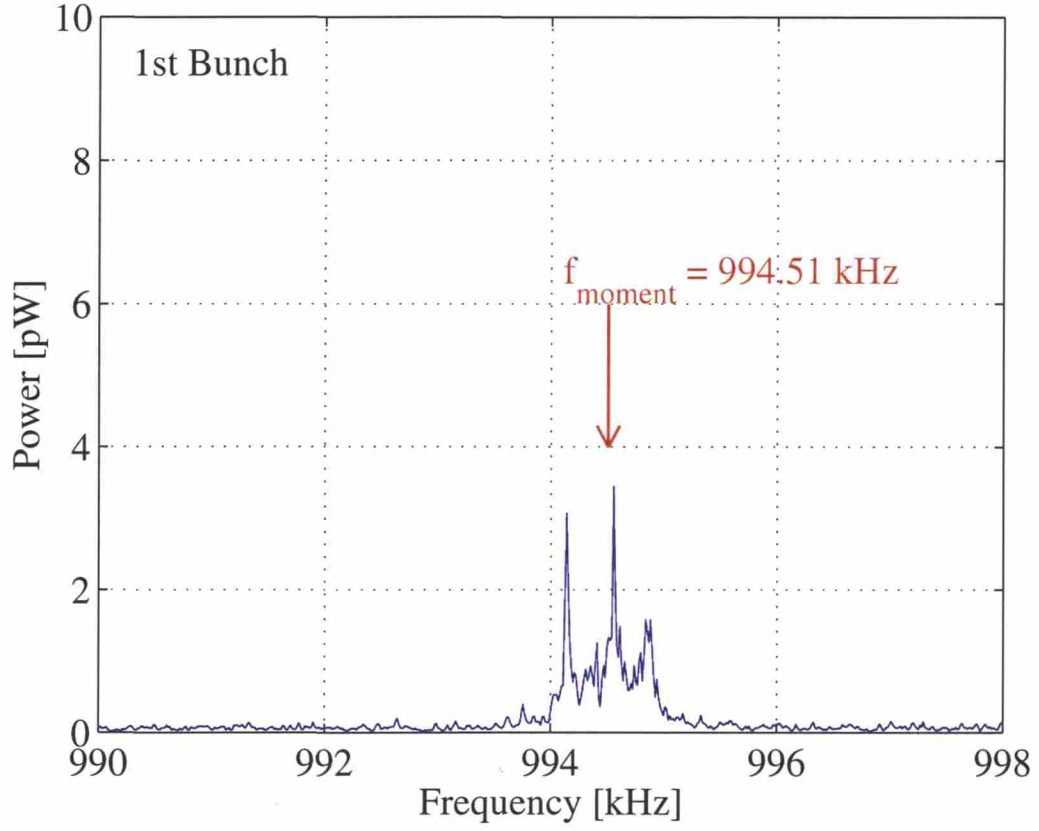


Figure 11: Spectrum of the 1st bunch in the 280-bunch train at $f_{\text{shutter}} + qf_{\text{rev}}$. The red arrow designates the frequency of the first-order moment of the spectrum.

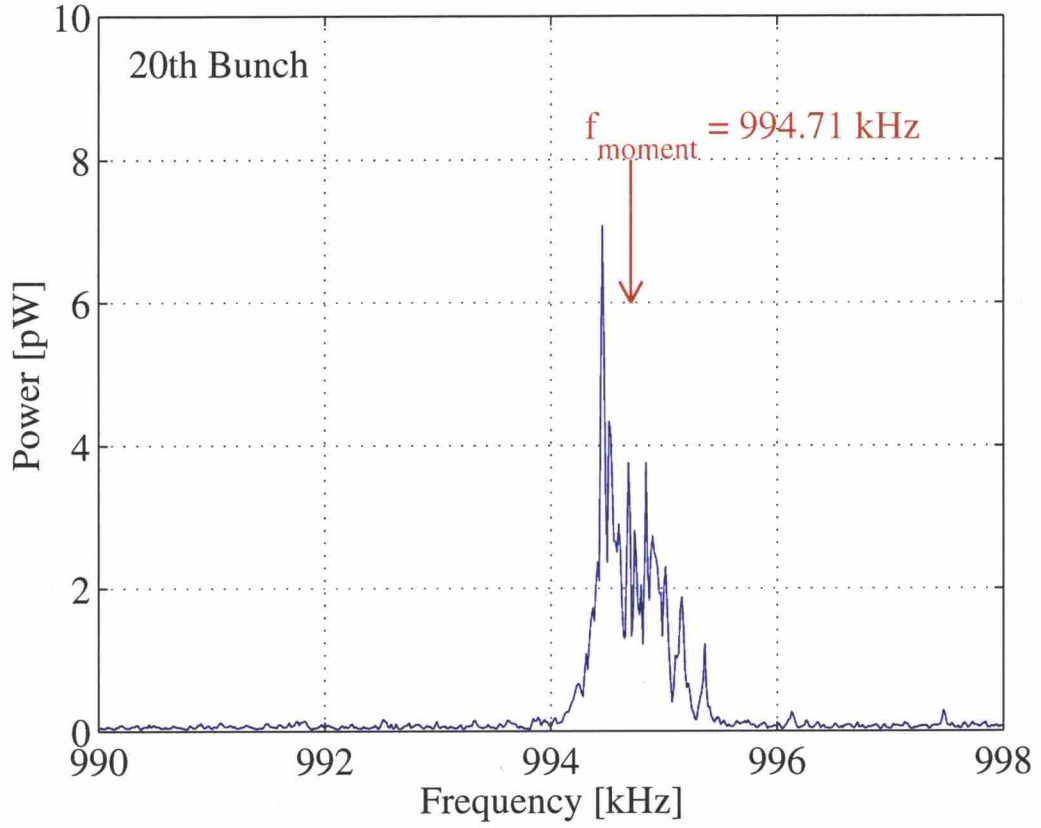


Figure 12: Spectrum of the 20th bunch in the 280-bunch train at $f_{\text{shutter}} + qf_{\text{rev}}$. The red arrow designates the frequency of the first-order moment of the spectrum.

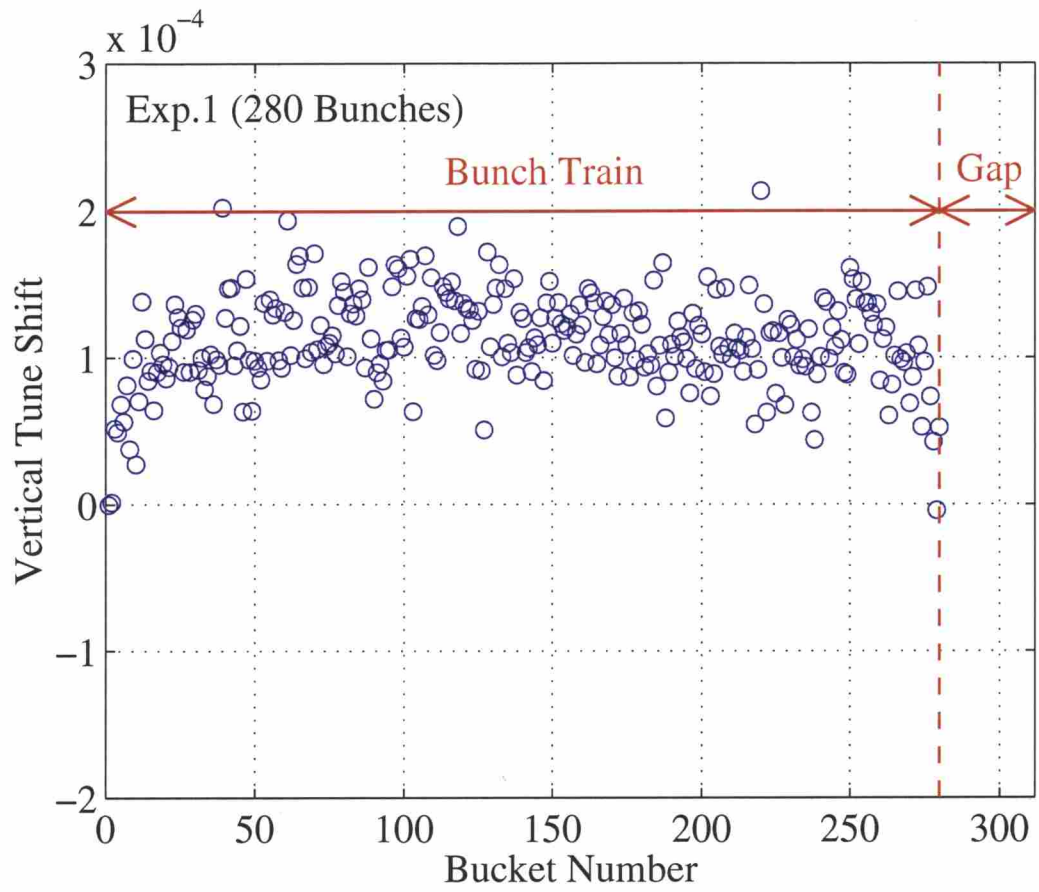


Figure 13: Vertical tune shifts of individual bunches along a bunch train with 280 bunches.

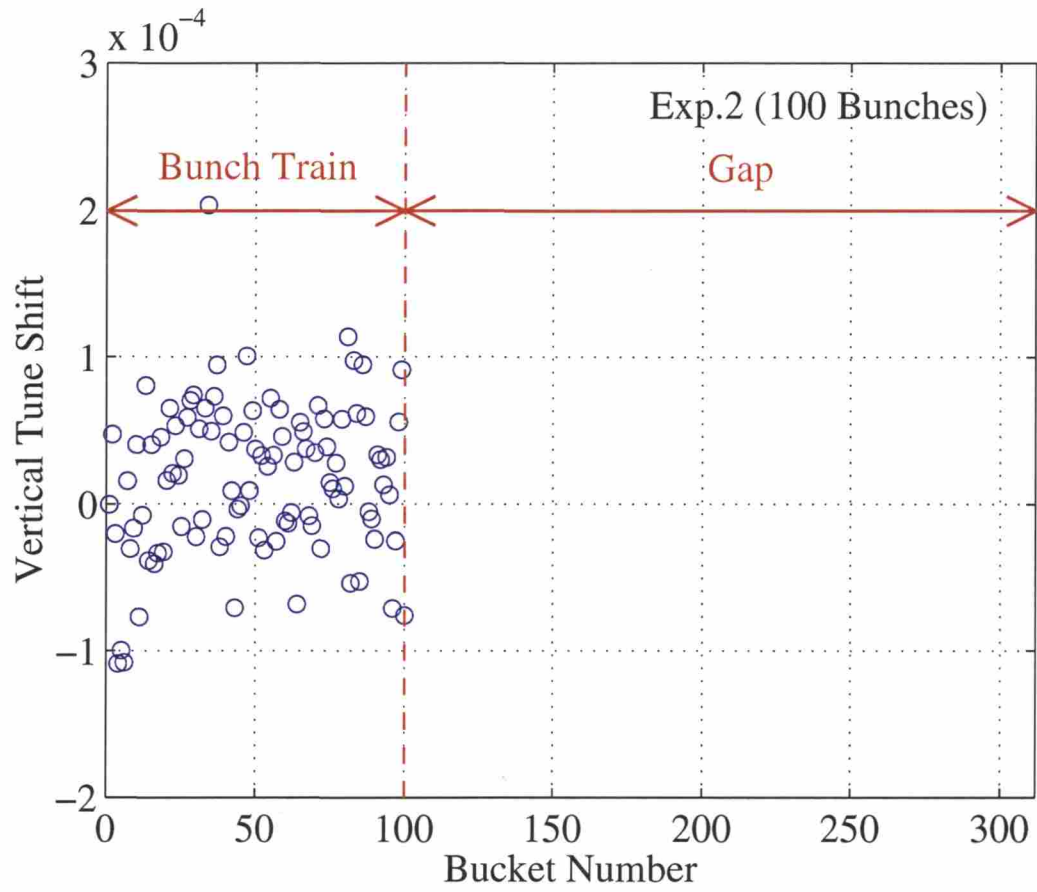


Figure 14: Vertical tune shifts of individual bunches along a bunch train with 100 bunches.

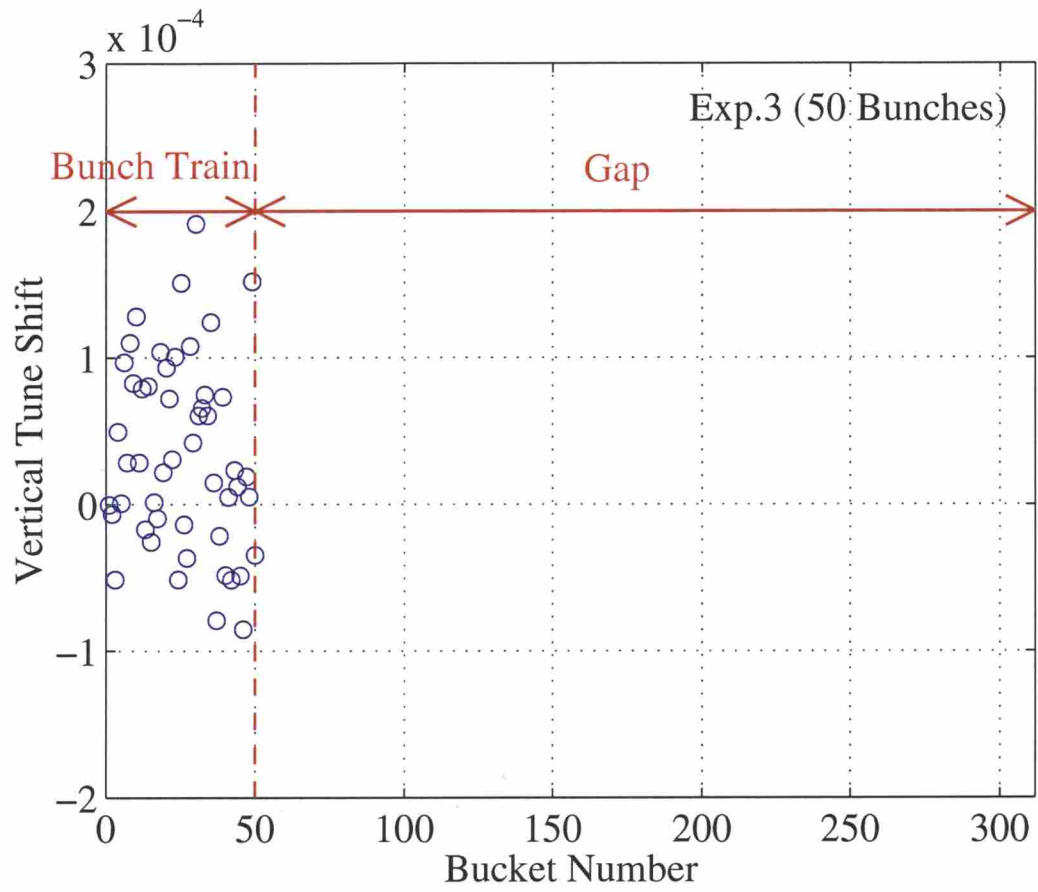


Figure 15: Vertical tune shifts of individual bunches along a bunch train with 50 bunches.

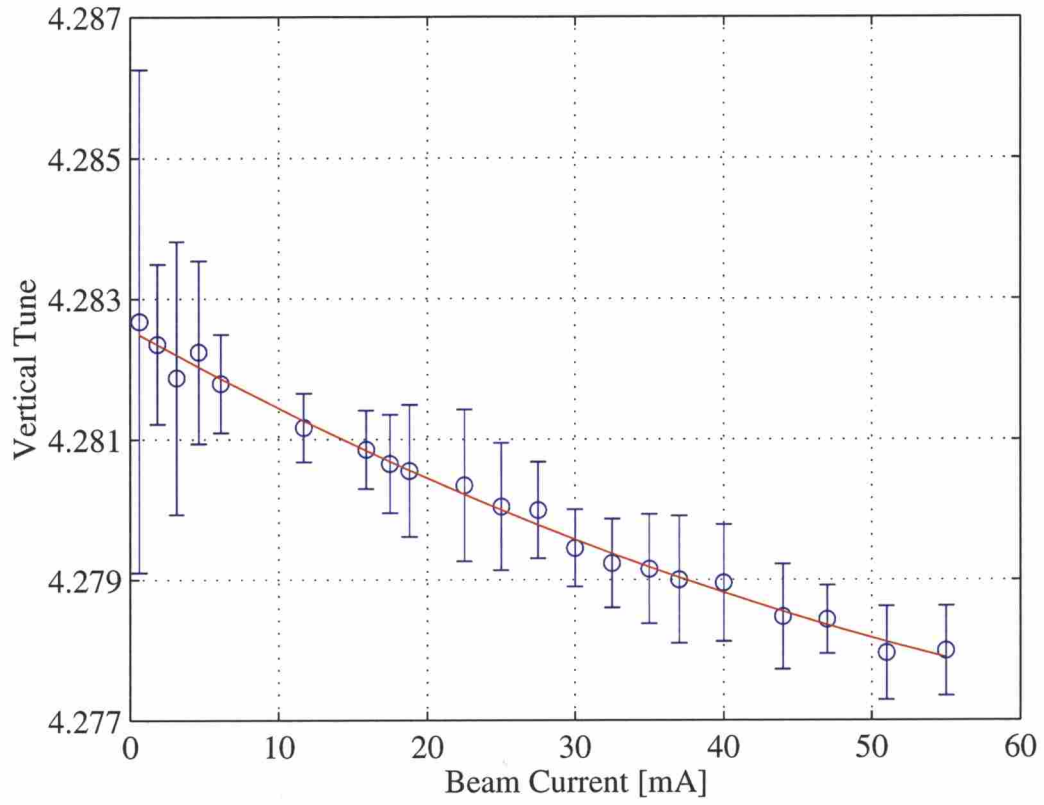


Figure 16: Dependence of the vertical tune on the beam current. The circles and the curve correspond to the experimental results and the fitted curve, respectively.

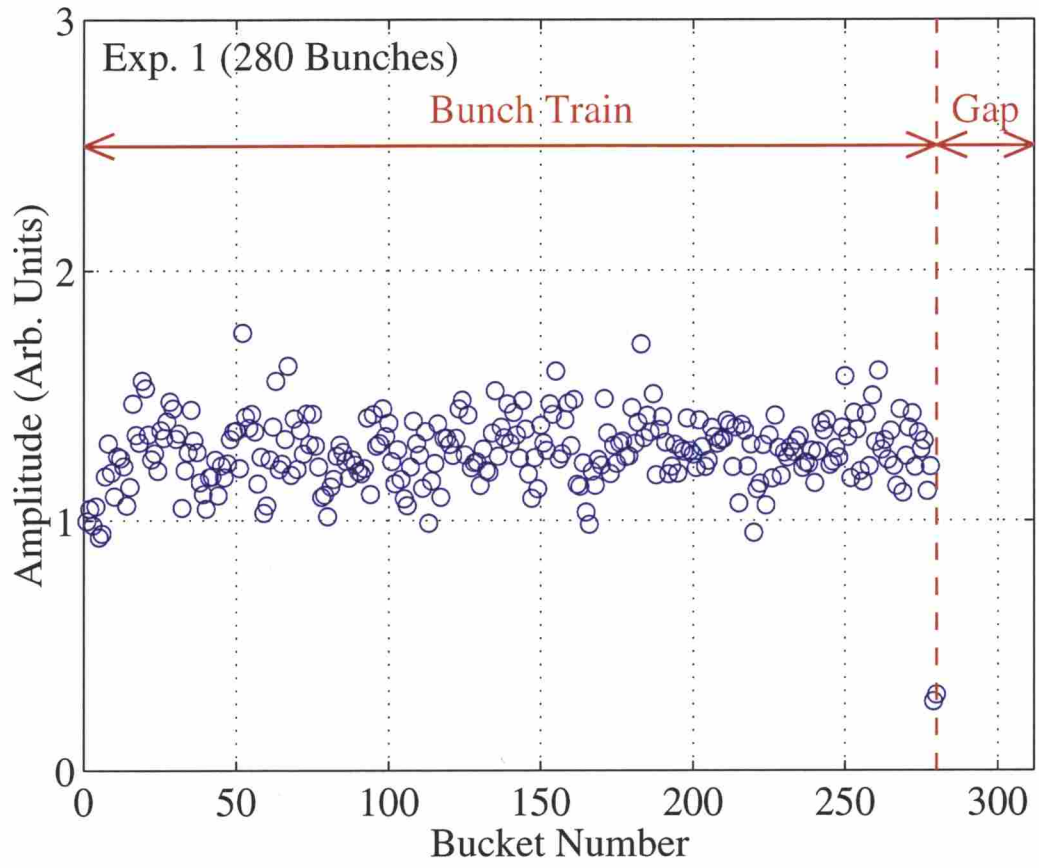


Figure 17: Oscillation amplitudes of individual bunches along a bunch train with 280 bunches.

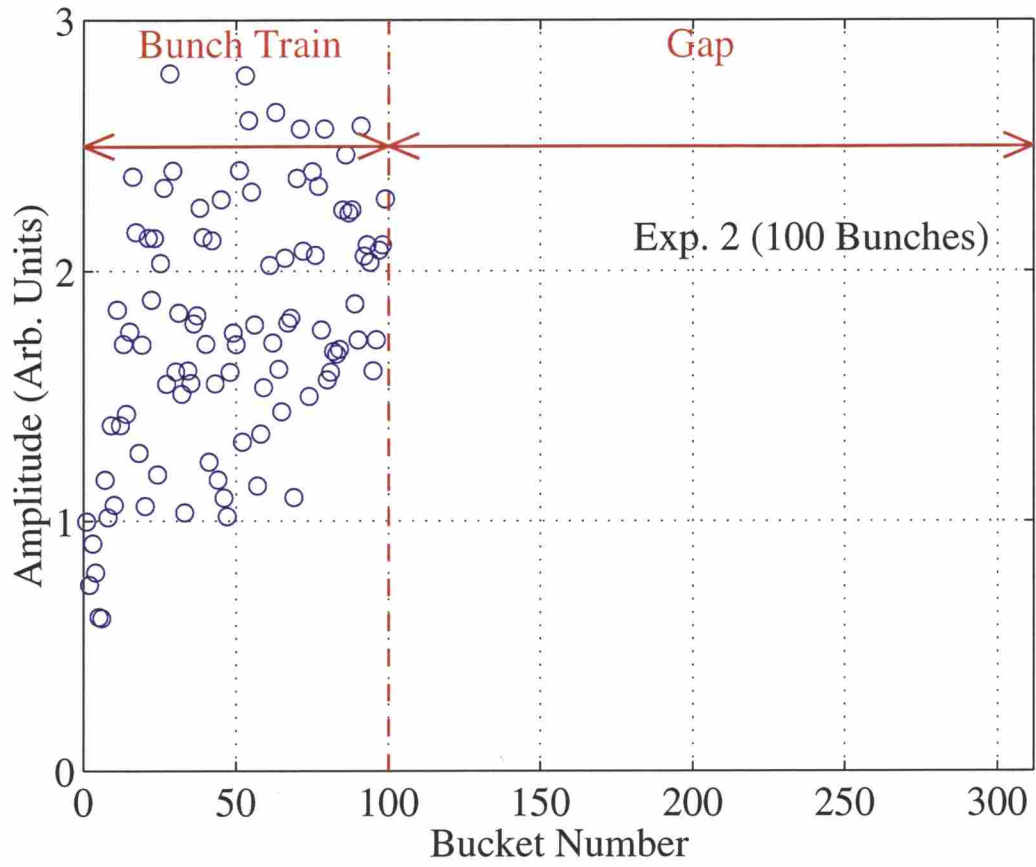


Figure 18: Oscillation amplitudes of individual bunches along a bunch train with 100 bunches.

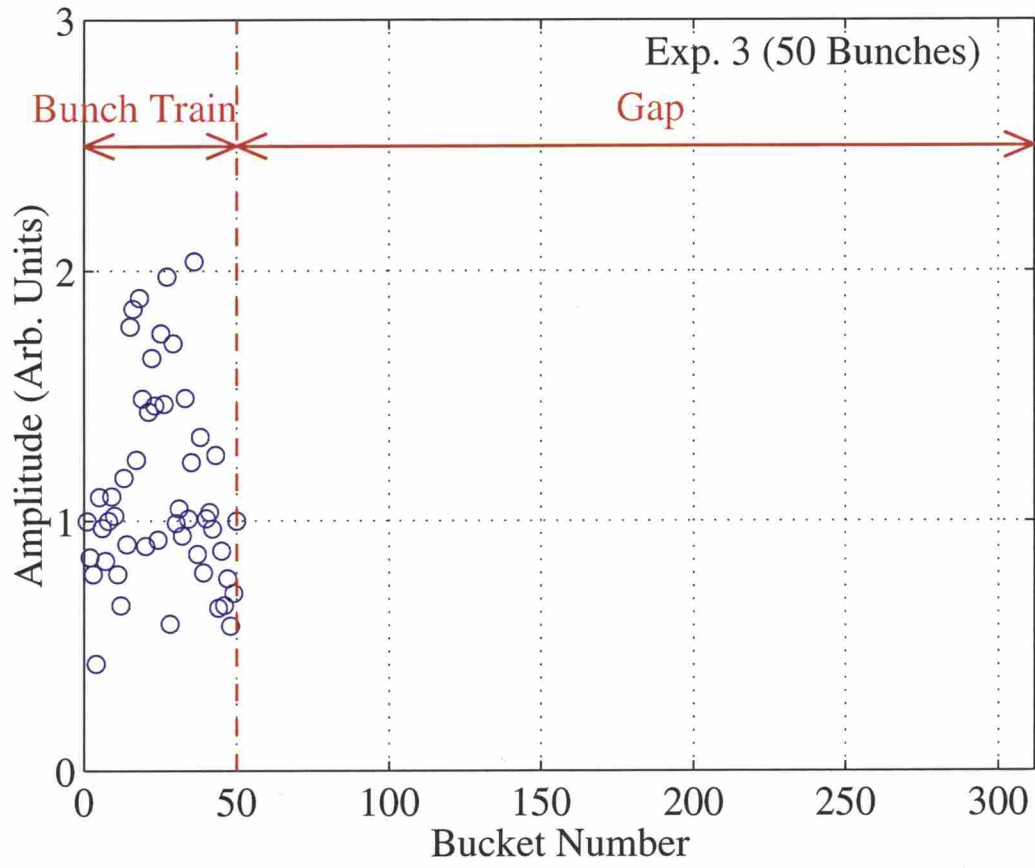


Figure 19: Oscillation amplitudes of individual bunches along a bunch train with 50 bunches.

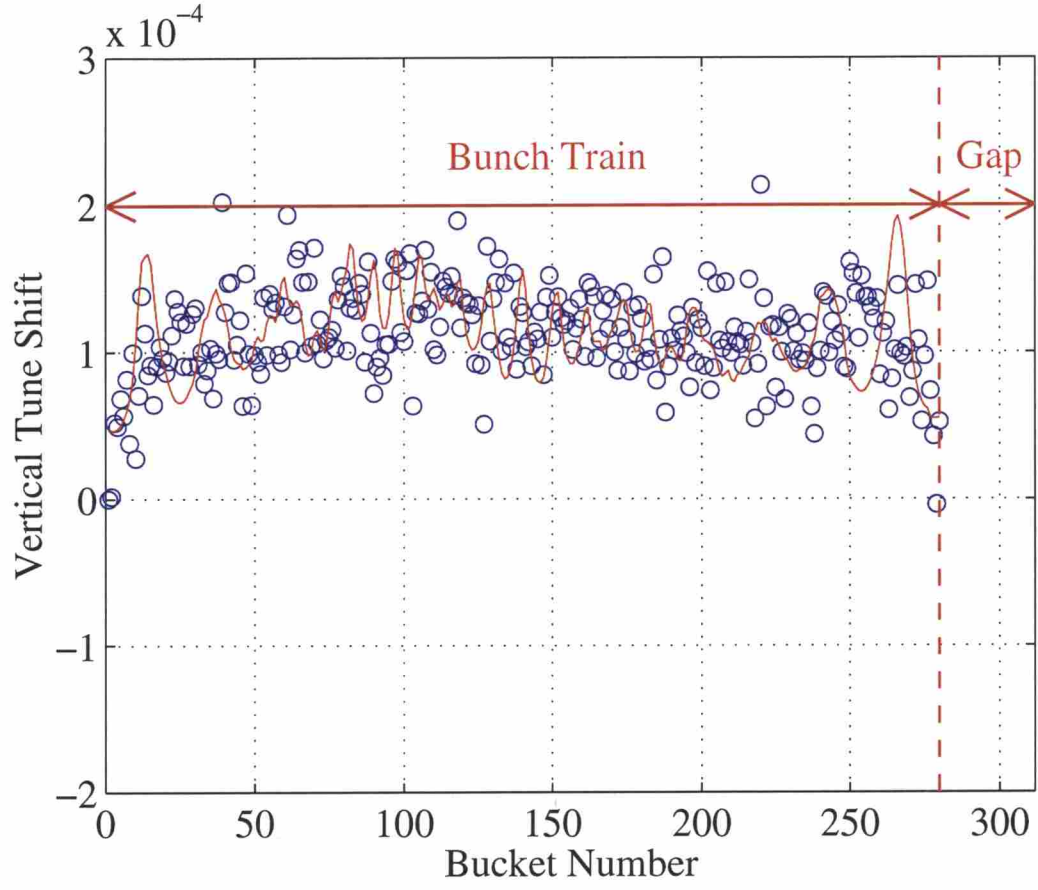


Figure 20: (Color) The change in the tunes along a 280-bunch train. The blue circles and the red curve correspond to the experimental results and the theoretical values, respectively.

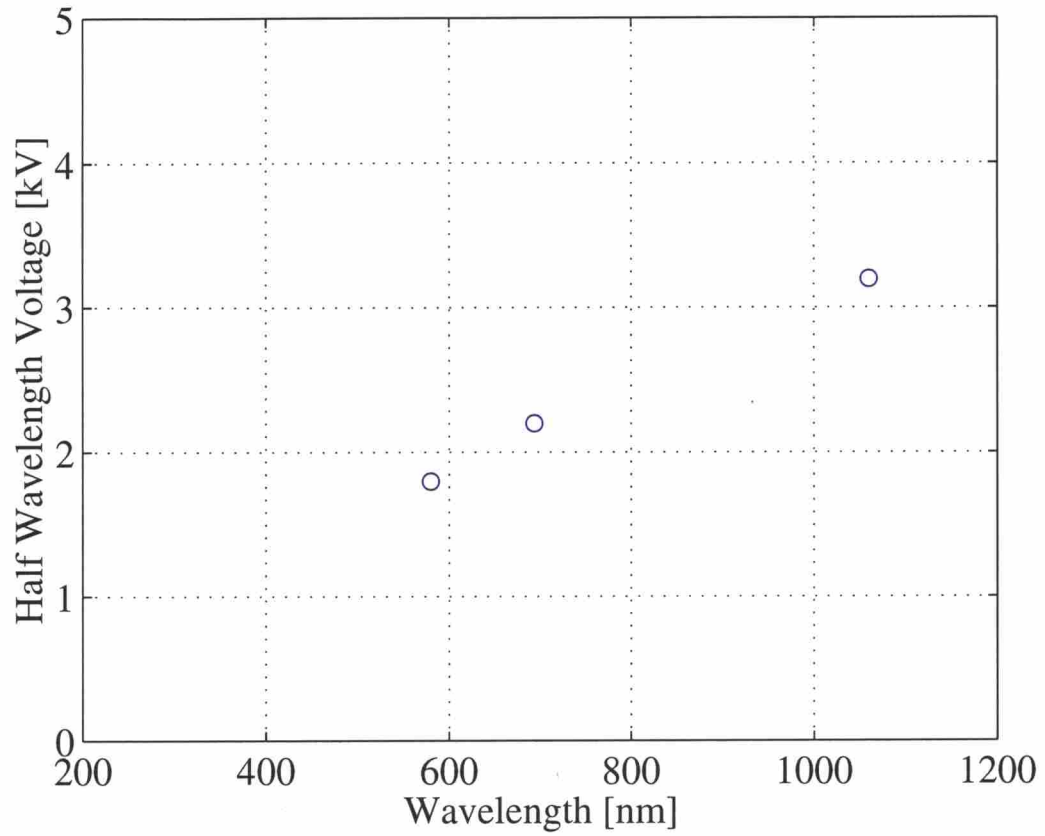


Figure 21: Dependence of the half wavelength voltage on the wavelength of the incident light. The figure comes from a data table of the pockels cell (Fastpulse Technology, 1044-FW).

Curriculum Vitae

1996 March, Bachelor at College of Natural Science, University of Tsukuba

1998 March, Master Degree at Doctoral Program in Physics, University of Tsukuba

Publications

1. A. Mochihashi *et al.*,
“Vertical Instability with Transient Characteristics in KEK-Photon
Factory Electron Storage Ring”,
submitted to Physical Review Special Topics, Accelerators and Beams.
2. A. Mochihashi *et al.*,
“Observation of Transverse Instability Using Bunch-by-Bunch Beam
Diagnostic System in KEK-PF”,
Proc. of the 7th European Particle Accelerator Conference, Vienna
(2000).
3. T. Obina *et al.*,
“Vertical Instability with Transient Characteristics Observed in KEK-
PF”,
Proc. of the 7th European Particle Accelerator Conference, Vienna
(2000).
4. A. Mochihashi *et al.*,
“Observation of Transverse Instabilities Using Bunch-by-Bunch Beam
Diagnostic System in KEK-PF”,
Proc. of the 12th Symposium on Accelerator Science and Technology,
Wako, Saitama, Japan (1999).

5. A. Mochihashi, K. Sato,
“Analytical Expression of Transient Eddy Current Effect in Iron-Solid Magnets”,
Proc. of 15th International Conference on Cyclotrons and Their Applications, Centre de Congrès, Caen, France (1998).

Presentations

1. A. Mochihashi *et al.*,
“Observation of Beam Instability Using Bunch-by-Bunch Beam Diagnostic System in KEK-PF”,
Meeting of the Physical Society of Japan, Kinki University, March (2000).